

PHASE RETRIEVAL WITH BACKGROUND INFORMATION: DECREASED REFERENCES AND EFFICIENT METHODS

ZIYANG YUAN*, HAOXING YANG[†], NINGYI LENG[‡], AND HONGXIA WANG[§]

Abstract. Fourier phase retrieval(PR) is a severely ill-posed inverse problem that arises in various applications. To guarantee a unique solution and relieve the dependence on the initialization, background information can be exploited as a structural priors [1]. However, the requirement for the background information may be challenging when moving to the high-resolution imaging. At the same time, the previously proposed projected gradient descent(PGD) method also demands much background information.

In this paper, we present an improved theoretical result about the demand for the background information, along with two Douglas Rachford(DR) based methods. Analytically, we demonstrate that the background required to ensure a unique solution can be decreased by nearly 1/2 for the 2-D signals compared to the 1-D signals. By generalizing the results into d -dimension, we show that the length of the background information more than $(2^{\frac{d+1}{d}} - 1)$ folds of the signal is sufficient to ensure the uniqueness. At the same time, we also analyze the stability and robustness of the model when measurements and background information are corrupted by the noise. Furthermore, two methods called Background Douglas-Rachford (BDR) and Convex Background Douglas-Rachford (CBDR) are proposed. BDR which is a kind of non-convex method is proven to have the local R-linear convergence rate under mild assumptions. Instead, CBDR method uses the techniques of convexification and can be proven to own a global convergence guarantee as long as the background information is sufficient. To support this, a new property called F-RIP is established. We test the performance of the proposed methods through simulations as well as real experimental measurements, and demonstrate that they achieve a higher recovery rate with less background information compared to the PGD method.

Key words. Fourier phase retrieval, Background information, Uniqueness, Douglas-Rachford method

AMS subject classifications. 12D05, 49N30, 49N45, 90C26

1. Introduction. The Fourier PR problem, which aims to recover a signal from its intensity only Fourier spectrum, arises in a variety of applications such as X-ray crystallography, astronomy, coherent diffraction imaging(CDI) and Fourier ptychography[2, 3, 4].

1.1. Problem formulation. Mathematically, the 1-D discrete Fourier PR can be formulated as

$$(1.1) \quad \begin{aligned} & \text{Find } \mathbf{x} \in \mathbb{C}^n \\ & \text{s.t. } |\mathbf{F}_i^H \mathbf{x}|^2 = b_i, \quad i = 1, \dots, m, \end{aligned}$$

where $\{\mathbf{F}_i := [1, e^{\frac{2\pi j(i-1)}{m}}, \dots, e^{\frac{2\pi j(i-1)(n-1)}{m}}]^T, i = 1, \dots, m\}$ is the Fourier basis with $j = \sqrt{-1}$, $[\cdot]^H$ denotes the conjugate transpose. $\mathbf{b} = [b_1, b_2, \dots, b_m]^T$ is the measurement. In short, the Fourier PR problem is to recover the signal of interest \mathbf{x} from the intensity only Fourier spectrum \mathbf{b} .

*First author, Academy of Military Sciences, Beijing and Department of Mathematics, National University of Defense Technology, Changsha, Hunan, 410073, P.R.China.(yuanziyang11@nudt.edu.cn)

[†]Second author, Department of Mathematics, National University of Defense Technology, Changsha, Hunan, 410073, P.R.China. (saber1222@foxmail.com)

[‡]Third author, Department of Mathematics, National University of Defense Technology, Changsha, Hunan, 410073, P.R.China. (623567098@qq.com)

[§]Corresponding author, Department of Mathematics, National University of Defense Technology, Changsha, Hunan, 410073, P.R.China. Corresponding author.(wanghongxia@nudt.edu.cn)

It is evident that the solutions of (1.1) are not unique. For example, if $\mathbf{x}_1 = \mathbf{x}_2 e^{j\theta}$, where $\theta \in [0, 2\pi)$, then $|\mathbf{F}_i^H \mathbf{x}_1| = |\mathbf{F}_i^H \mathbf{x}_2|$, $i = 1, \dots, m$. Additionally, the conjugate transpose and circular shift of \mathbf{x} also yield the same measurements \mathbf{b} . Therefore, the uniqueness of the Fourier PR problem is considered up to these transformations which are called trivial solutions. Recent studies have focused on understanding the properties of the solutions and how to mitigate the effects caused by the non-trivialities[5, 6, 7, 8, 9].

1.2. Previous works. For the 1-D Fourier PR problem (1.1), it has been proven that there are at most 2^{n-1} different solutions up to a global phase when $m \geq 2n-1$ [9]. However, the results change for the problem in the multiple dimension. According to [10], if the dimension $d \geq 2$ and $m_i \geq 2n_i - 1, i = 1, \dots, d$, the uniqueness can be guaranteed except for a set of signals with zero measure, where n_i and m_i are the length of the signal and measurements respectively in each dimension. This sheds light on the applications of the 2-D Fourier PR problem. A series of algorithms has been subsequently been developed. Representatives are the alternating projection or reflection methods such as GS method, HIO method, RAAR method and ADMM method.[11, 12, 13, 14, 15]. These methods update iterations by projection or reflection between different domains. However, these methods are liable to stagnate namely iterations generated by the algorithms stagnate before converging to the neighbor of the ground truth especially when the measurements are corrupted by the noise. At the same time, although many theoretical and algorithmic results about PR for the general frames¹ have made a great progress[6, 16, 17, 18], these works usually fail when dealing with the Fourier PR problem. They are instructive but cannot be applied to the Fourier PR problem directly.

Utilizing priors is one of the efficient ways to constrain the feasible solutions and relieve the illness of the Fourier PR problem. For instance, additional information about the unknown signal may be helpful to guarantee the unique solution [19, 20, 21]. Sparsity is one of the widely used priors. It has been shown in [22] that the full auto-correlation series of a 1-D s -sparse real signal² \mathbf{x} is sufficient to uniquely determine \mathbf{x} as long as $s \neq 6$ and the auto-correlation sequence is collision free³. In addition, if m is a prime, [23] proves that $m \geq s^2 - s + 1$ measurements are sufficient to uniquely determine the auto-correlation series of \mathbf{x} . For the d -dimension signal $\mathbb{R}^{n \times \dots \times n}$, under the condition that the support of the signal is distributed as the Gaussian process, [24] proves that the signal can be recovered from the auto-correlation function of the signal with high probability as long as the sparsity is at most $\mathcal{O}(n^{d\theta})$ for any $\theta < \frac{1}{2}$. Meanwhile, a large number of highly efficient optimization algorithms are come up to deal with the sparse Fourier PR problem [25, 26, 27]. Interested readers can refer to [5, 8] for a comprehensive reviews about the different priors which may enforce the Fourier PR problem to be unique. In [19, 28], they attempt to use interference with a known or unknown reference signal to achieve the uniqueness of the Fourier PR problem. In [29], they propose a general mathematical framework and recovery algorithm for the PR problem under different references. Notice that in [30], it uses the deep neural network to learn a data-adaptive reference so that algorithm proposed can perform better.

¹General frames here mean the transforming vectors $\mathbf{F}_i, i = 1, \dots, m$ in (1.2) are not orthogonal basis but a kind of frames.

² s -sparse signal means there are up to s nonzero elements in a signal.

³A signal $\mathbf{x} \in \mathbb{R}^n$ is said to be collision free if for any distinct $i_1, i_2, i_3, i_4 \in 1, 2, \dots, n$, we have $x_{i_1} - x_{i_2} \neq x_{i_3} - x_{i_4}$.

While a series of priors have been introduced, most of them only guarantee uniqueness up to trivial solutions. This means that it is impossible to distinguish \mathbf{x} from its trivial ambiguities, which significantly degrades the quality of the reconstruction. Therefore, more efficient priors are required to eliminate this issue. In [1], a model that utilizes background information is proposed as follows:

$$(1.2) \quad \begin{aligned} & \text{Find } \mathbf{z} \in \mathbb{C}^{n+k} \\ & \text{s.t. } |\mathbf{F}_i^H \mathbf{z}|^2 = b_i, \quad i = 1, \dots, m, \\ & \quad z_{n+l} = y_l, \quad l = 1, \dots, k, \end{aligned}$$

where $\mathbf{y} \in \mathbb{R}^k$ represents the background information that is known in advance. Utilizing this information, the uniqueness of Fourier PR can be guaranteed if $k \geq 3n - 1$, $y_l \stackrel{i.i.d.}{\sim} \mathcal{N}(0, \sigma^2)$, where $\sigma^2 > 0$, and $l = 1, 2, \dots, k$. It should be noted that the solution here is **exactly unique**. Numerical tests have shown that the projected gradient descent (PGD) method can recover the ground truth without requiring an elaborate initialization and is robust to the noisy measurements. However, the demand for the background information about $3n$ is still large in the practical applications, especially when the dimension is high. Recall that for the Fourier PR problem with dimension d , $m_i \geq 2n_i - 1, i = 1, 2, \dots, d$ is required to ensure uniqueness up to the trivial solutions [9]. However, according to [31], samples less than $2n_i - 1, i = 1, 2, \dots, d$ is also sufficient, and $m_i \geq 2^{\frac{1}{d}} n_i, i = 1, 2, \dots, d$ can work in practice. This conjecture hints us to utilize the correlations between different dimensions to lower the demand of background information.

1.3. Works in this paper. This paper presents theories about the uniqueness, stability and robustness of (1.2). These results require less background information compared to [1]. Additionally, we also propose two new methods that guarantee local and global convergence respectively. Meanwhile, numerical simulations and optical experiments demonstrate the efficiency of the proposed methods. Specifically, works in this paper can be classified into four main aspects.

- Firstly, we prove the uniqueness of the solution for (1.2) in the 2-dimension situation namely ground truth $\mathbf{X} \in \mathbb{R}^{n_1 \times n_2}$. Specifically, we show that $(n_1 + k_1)(n_2 + k_2) \geq (2n_1 - 1)(3n_2 - 1) + n_2$ ensures the uniqueness when each element of the background \mathbf{Y} satisfies the normal distribution, where k_1 and k_2 represent the length of the background in two directions, respectively. Furthermore, we generalize the results into d -dimension and prove that

$$\prod_{i=1}^d (n_i + k_i) \geq 2 \prod_{i=1}^d n_i + \prod_{i=1}^d (2n_i - 1), \quad i = 1, 2, \dots, d,$$

is sufficient to guarantee the uniqueness. These results also develop the theories of affine Fourier phase retrieval, which can be seen in Table 1.

- Secondly, we prove the stability of (1.2) in the 2-dimension situation, specifically

$$C_1 \|\mathbf{X}_1 - \mathbf{X}_2\|_F \leq \|\text{vec}(\mathbf{I}_1) - \text{vec}(\mathbf{I}_2)\|_2 \leq C_2 \|\mathbf{X}_1 - \mathbf{X}_2\|_F,$$

where C_1 and C_2 are constants determined by n_1, n_2 and \mathbf{Y} . \mathbf{I}_1 and \mathbf{I}_2 are the intensity-only measurements generated by \mathbf{X}_1 and \mathbf{X}_2 with the same \mathbf{Y} . Moreover, the error bound of the distance between the estimation \mathbf{X}^* and

the ground truth \mathbf{X} is also derived when the background information and intensity-only measurements are corrupted by the noise ε_1 and ε_2 respectively and $\tilde{\mathbf{Y}}$ and $\tilde{\mathbf{I}}$ are known:

$$\|\mathbf{X}^* - \mathbf{X}\|_F \leq C_1(c_1, c_2) + C_2(c_2)\|\text{vec}(\tilde{\mathbf{Y}})\|_1 + \sqrt{C_3(c_2)\|\text{vec}(\tilde{\mathbf{I}})\|_1} + C_4(c_1, c_2),$$

where c_1 and c_2 are the noise levels of ε_1 and ε_2 satisfying $\|\varepsilon_1\|_\infty \leq c_1$ and $\|\varepsilon_2\|_\infty \leq c_2$, and $C_1(c_1, c_2)$, $C_2(c_2)$, $C_3(c_2)$, $C_4(c_1, c_2)$ are constants determined by c_1 and c_2 .

- Next, to improve the performance of the PGD method when the background information is insufficient, a method called the Background Douglas Rachford(BDR) is proposed. Theoretical results demonstrate that it can escape the fixed points of the method, which may not be the ground truth. Furthermore, under mild assumptions, we prove that the BDR method has an R-linear convergence rate if the initialization is close to the ground truth
- At the same time, we also use convex relaxation techniques, transforming (1.2) into a convex problem (3.4). Theoretical results show that (3.4) and (1.2) can keep the same solution with probability 1 as if background information is sufficient. To demonstrate this, a property called Fourier Spectrum Restricted Isometry Property (F-RIP) is established.

$$(c_1(n, k, \mathbf{x}) - \delta)\|\mathbf{h}\|_2^2 \leq \frac{1}{k}\|\mathbf{L}_1\mathbf{h}\|_2^2 \leq (c_2(n, k, \mathbf{x}) + \delta)\|\mathbf{h}\|_2^2, \forall \mathbf{h} \in \mathbf{C}_2,$$

where $c_1(n, k, \mathbf{x})$ and $c_2(n, k, \mathbf{x})$ are two constants depending on n, k and ground truth, $c_1(n, k, \mathbf{x}) > \delta$, $\mathbf{C}_2 = \{\mathbf{h} \in \mathbb{R}^{n+k} \mid \|\mathbf{F}_i^H \mathbf{h}\|^2 \leq 4, i = 1, \dots, n+k\}$, and $\mathbf{L}_1 \in \mathbb{R}^{k \times (n+k)}$ is a special partial random circulant matrix where part of the variables in \mathbf{L}_1 are determined. Additionally, we introduce the Convex Background Douglas Rachford (CBDR) method for solving the convex problem (3.4), which has a guaranteed global convergence.

- Last, through numerous tests including simulated Fourier measurements and optical Charge-coupled Device(CCD) measurements, we have verified the high efficiency of the newly proposed methods which require less background information to achieve a higher successfully rate compared to the PGD method.

In this article, bold uppercase and lowercase letters represent matrices or sets and vectors respectively. $|\cdot|$ denotes the module of a number, the determinant of matrix or the cardinality of a set. The notation $\text{vec}(\cdot)$ represents the vectorizing operation, while \odot denotes the Hadamard product and \otimes represents the Kronecker product. The abbreviation i.i.d stands for 'independent and identically distributed', and $\|\cdot\|_F$ is the Frobenius norm. The symbol $\|\cdot\|_1$ denotes the 1-norm of a vector or matrix. \mathbf{B}_1^{n+k} is the ℓ_1 Ball in \mathbb{R}^{n+k} , and \mathbf{B}_2^{n+k} is the ℓ_2 Ball in \mathbb{R}^{n+k} .

2. Theoretical Analysis of the model. For the sake of brevity, we only analyze the problem when the signal of interest is real, but the complex situation can be generalized. The theoretical analysis is specialized to the multi-dimension array, thus we don't use the same notations as in [1].

2.1. Uniqueness of the solution. The physical setup for the phase retrieval with background information, as studied in this paper, is depicted in Figure 1. An unknown sample $\mathbf{X} \in \mathbb{R}^{n_1 \times n_2}$ is centered on a reference $\mathbf{Y} \in \mathbb{R}^{(n_1+k_1) \times (n_2+k_2)}$. The region of the reference that overlaps with the sample is transparent, i.e., $\mathbf{Y}|_\Omega = \mathbf{0}$ where Ω is the support of \mathbf{X} and is known in advance. The reference object can be an

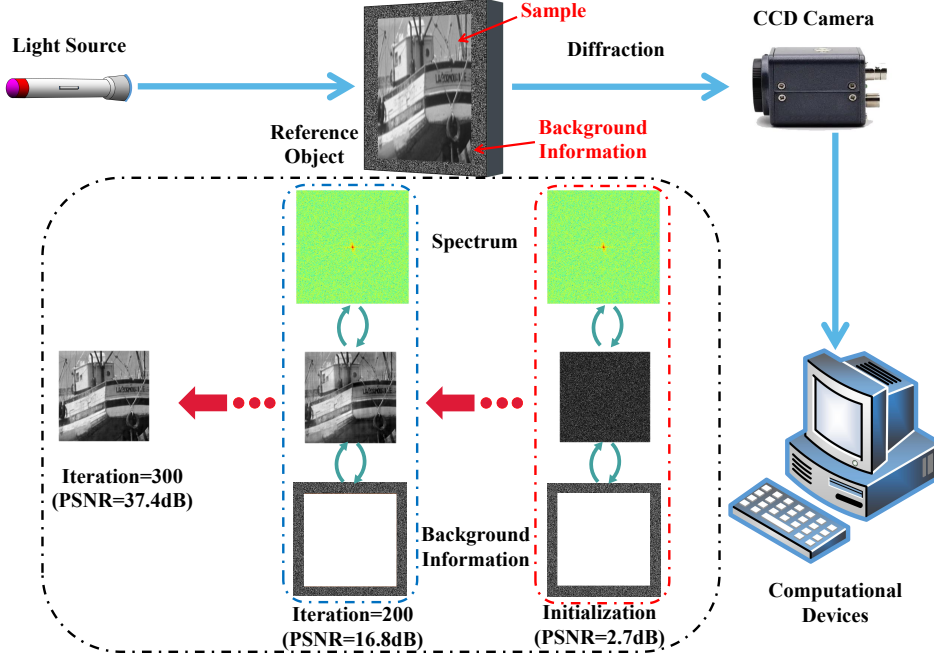


Fig. 1: Procedure of phase retrieval with background information, where PSNR stands for the Peak Signal to Noise Ratio.

SLM (Spatial Light Modulator), which is set to modulate the light passing through the overlapped area. The CCD records only the phase-free intensity $\mathbf{I} \in \mathbb{R}^{m_1 \times m_2}$ which is the diffraction pattern resulting from the combination of \mathbf{X} and \mathbf{Y} .

If we denote the combination of \mathbf{X} and \mathbf{Y} as $\mathbf{Z} \in \mathbb{R}^{(n_1+k_1) \times (n_2+k_2)}$, that is to say,

$$\mathbf{Z}_{i,h} = \begin{cases} \mathbf{X}_{i,h}, & (i, h) \in \Omega \\ \mathbf{Y}_{i,h}, & \text{otherwise.} \end{cases},$$

then the mathematical model of the PR problem with background information can be formulated as:

$$(2.1) \quad \begin{aligned} & \text{Find } \mathbf{Z} \\ & \text{s.t. } \left| \mathbf{F}_{(n_1+k_1) \times m_1}^H \mathbf{Z} \mathbf{F}_{m_2 \times (n_2+k_2)}^H \right|^2 = \mathbf{I} \\ & \mathbf{Z}_{i,h} = \begin{cases} \mathbf{X}_{i,h}, & (i, h) \in \Omega \\ \mathbf{Y}_{i,h}, & \text{otherwise} \end{cases}, \end{aligned}$$

where $\mathbf{F}_{(n_1+k_1) \times m_1}^H \in \mathbb{C}^{m_1 \times (n_1+k_1)}$ and $\mathbf{F}_{m_2 \times (n_2+k_2)}^H \in \mathbb{C}^{(n_2+k_2) \times m_2}$ are sub-matrices extracted separately from Fourier matrices $\mathbf{F}_{m_1 \times m_1}^H$ and $\mathbf{F}_{m_2 \times m_2}^H$.

The generalization of the theorem in [1] states that if one of the following two conditions is satisfied, then (2.1) can guarantee the exact uniqueness of the solution namely excluding all trivial ambiguities.

1. $m_1 \geq 2(n_1 + k_1) - 2$, $k_1 \geq n_1$, $k_2 \geq 0$ and $\mathbf{Z}_{n_1+k_1,h} \neq 0$, $h = 0, \dots, n_2 - 1$.

2. $m_1 = n_1 + k_1 + p$, $p \geq 0$, $k_2 \geq 0$,

$$k_1 \geq \begin{cases} \max(3n_1 - 2 - p, n_1), & m_1 - 2n_1 + 1 \text{ is odd} \\ \max(3n_1 - 1 - p, n_1), & m_1 - 2n_1 + 1 \text{ is even} \end{cases}$$

and $\mathbf{Y}_{i,h} \stackrel{i.i.d.}{\sim} \mathcal{N}(\mu, \sigma^2)$, $\sigma^2 > 0$, $(i, h) \notin \Omega$.

When there is no oversampling, i.e., $m_1 = n_1 + k_1$, the result above shows that k_1 should be at least 3 times as large as n_1 . This requirement may exceed the resolution of CCD in practice especially when n_1 is large. Note that there are no extra requirements for k_2 . Intuitively, we can constrain k_2 by utilizing the correlations of \mathbf{X} along two directions, which can reduce the requirement for the background information. As stated in [1], oversampling can generally decrease the requirements for the background information. Thus, Theorem 2.1 only consider the worst-case scenario when $m_i = n_i + k_i$, $i = 1, 2$.

THEOREM 2.1. *Consider model (2.1) with $\mathbf{Y}_{i,h} \stackrel{i.i.d.}{\sim} \mathcal{N}(\mu, \sigma^2)$ and $\sigma > 0$. If $(n_1 + k_1)(n_2 + k_2) \geq (2n_1 - 1)(3n_2 - 1) + n_2$, the unique solution of (2.1) can be guaranteed. Especially, if $n = n_1 = n_2$ and $k = k_1 = k_2$, then $k \geq (\sqrt{6} - 1)n \approx 1.45n$ is sufficient.*

Remark 2.2. Comparing to the traditional Fourier PR problem, although the number of measurements required to guarantee the uniqueness of (2.1) is not reduced, namely, $m_i \geq \sqrt{6}n_i \geq 2n_i - 1$, $i = 1, 2$, the solution can be free from trivial ambiguities. This usually makes methods easier to find the ground truth. Additionally, it is worth noting that (2.1) is a special case of the affine phase retrieval problem, achieved by splitting \mathbf{Z} into \mathbf{X} and \mathbf{Y} . The 1-D affine phase retrieval problem is formulated as follows:

$$(2.2) \quad \begin{aligned} & \text{Find } \mathbf{x} \\ & \text{s.t. } \mathbf{b} = |\mathbf{A}^H \mathbf{x} + \mathbf{d}|^2, \end{aligned}$$

where $\mathbf{A} \in \mathbb{C}^{n \times m}$ is the measurement matrix, $\mathbf{b} \in \mathbb{R}^m$ and $\mathbf{d} \in \mathbb{C}^m$ are known in advance. There are several studies that investigate the uniqueness of (2.2) under different conditions. Some of these results are summarized in Table 1. It can be observed that the affine phase retrieval problem is guaranteed to be unique if $m \geq 4n$, regardless of whether the measurements are general or Fourier.

Before proving Theorem 2.1, some preliminaries will be introduced. Let $m_i = n_i + k_i$, $i = 1, 2$. First, the 2-D circular auto-correlation series of $\mathbf{X} \in \mathbb{R}^{n_1 \times n_2}$ is defined as:

$$(2.3) \quad \mathbf{R}_{l_1, l_2} := \text{vec}(\mathbf{X}(-l_1, -l_2))^T \text{vec}(\mathbf{X}), 0 \leq l_1 \leq m_1 - 1, 0 \leq l_2 \leq m_2 - 1,$$

where $\text{vec}(\mathbf{X})$ is the vectorization of \mathbf{X} obtained by stacking each row of \mathbf{X} , and \mathbf{R}_{l_1, l_2} is the element in the l_1 th row and l_2 th column of \mathbf{R} . Furthermore, $\mathbf{X}_{i,h}(-l_1, -l_2) = \mathbf{X}_{i-l_1, h-l_2} = \mathbf{X}_{i_1, h_1}$, $i_1 \in \{0, \dots, n_1 - 1\}$, $h_1 \in \{0, \dots, n_2 - 1\}$, $i - l_1 \equiv i_1 \pmod{m_1}$, $h - l_2 \equiv h_1 \pmod{m_2}$. The Wiener-Khinchin Theorem leads to the following lemma, which establishes a connection between \mathbf{R} and \mathbf{I} .

LEMMA 2.3. *For the problem shown in (2.1), the spectrum \mathbf{I} and circular auto-correlation function \mathbf{R} are related by the equation below:*

$$(2.4) \quad \mathbf{F}_{m_2 \times m_2}^H \mathbf{R} \mathbf{F}_{m_1 \times m_1}^H = \mathbf{I}.$$

Table 1: Summary of uniqueness results. It should be noted that the uniqueness of the phase retrieval problem refers to uniqueness up to trivial solutions. However, for affine phase retrieval, uniqueness means that the solution is exactly unique.

	Type of the signal	Phase retrieval	Affine phase retrieval
General measurement	$\mathbf{x} \in \mathbb{R}^n$	$m \geq 2n - 1$, a full-spark random $\mathbf{A} \in \mathbb{R}^{m \times n}$ guarantees uniqueness with high probability[16]	$m \geq 2n + 1$, a generic $(\mathbf{A}, \mathbf{d}) \in \mathbb{R}^{m \times (n+1)}$ is sufficient to guarantee the uniqueness[32]
	$\mathbf{x} \in \mathbb{C}^n$	$m \geq 4n - 4$, a generic $\mathbf{A} \in \mathbb{C}^{m \times n}$ is sufficient to guarantee the uniqueness[33, 34]	$m \geq 4n + 1$, a generic $(\mathbf{A}, \mathbf{d}) \in \mathbb{C}^{m \times (n+1)}$ is sufficient to guarantee the uniqueness[32]
	s -sparse $\mathbf{x} \in \mathbb{R}^n (\mathbb{C}^n)$	$m \geq 4s - 1$ (or $8s - 2$), a generic $\mathbf{A} \in \mathbb{R}^{m \times n}$ (or $\mathbb{C}^{m \times n}$) is sufficient to guarantee the uniqueness[35]	$m \geq 2s + 1$ (or $4s + 1$), a generic $(\mathbf{A}, \mathbf{d}) \in \mathbb{R}^{m \times (n+1)}$ (or $\mathbb{C}^{m \times (n+1)}$) is sufficient to guarantee the uniqueness[32]
Fourier measurement	$\mathbf{x} \in \mathbb{C}^n$	No uniqueness[9]	$m \geq 4n - 1$, a generic $\mathbf{d} \in \mathbb{R}^m$ is sufficient to guarantee uniqueness[1]
	$\mathbf{x} \in \mathbb{C}^{n_1 \times \dots \times n_d}$ $d \geq 2$	$m_i \geq 2n_i - 1, i = 1, 2, \dots, d$ is sufficient to guarantee the uniqueness for real non-reducible signals[10]	$\prod_{i=1}^d m_i \geq 2 \prod_{i=1}^d n_i + \prod_{i=1}^d (2n_i - 1)$, a generic $\mathbf{d} \in \mathbb{C}^{m_1 \times m_2 \times \dots \times m_d}$, is sufficient to guarantee the uniqueness[This paper]

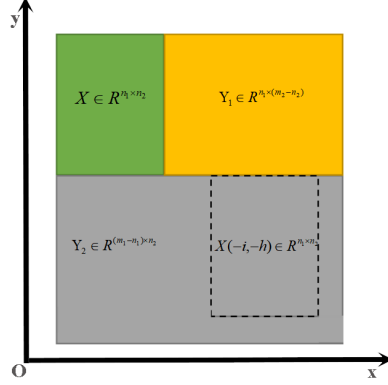
Now, we will prove Theorem 2.1. The main idea is to find sufficient linear combinations of the elements of \mathbf{X} from the circular auto-correlation matrix \mathbf{R} .

Proof of Theorem 2.1. By using Lemma 2.3, we can calculate \mathbf{R} from the 2-D inverse Fourier transform of \mathbf{I} . For the element in the i th row and h th column of \mathbf{R} , we have

$$(2.5) \quad \mathbf{R}_{i,h} = \text{vec}(\mathbf{Z}(-i, -h))^T \text{vec}(\mathbf{Z}).$$

With the aid of the known background information \mathbf{Y} , a series of linear combinations of $\text{vec}(\mathbf{X})$ can be obtained from (2.5). If these combinations are sufficient, then the uniqueness of solutions will be guaranteed. The remaining task is to determine how many linear combinations can be obtained from \mathbf{R} .

For better analysis, we divide \mathbf{Z} into three blocks: \mathbf{X} , \mathbf{Y}_1 and \mathbf{Y}_2 as shown in Figure 2 using three different colors. $\mathbf{Z}(-i, -h)$ is equivalent to shift \mathbf{X} by i units and h units along two directions namely $\mathbf{X}(-i, -h)$, which is the area surrounded by the dash line. If \mathbf{X} and $\mathbf{X}(-i, -h)$ do not overlap, the linear combinations of $\text{vec}(\mathbf{X})$ can be obtained from $\mathbf{R}_{i,h}$. Next, we will analyze the numbers of the linear combinations of $\text{vec}(\mathbf{X})$, assuming that \mathbf{X} and $\mathbf{X}(-i, -h)$ do not overlap.

Fig. 2: Three blocks in \mathbf{Z} .

Firstly, we assume that $\mathbf{X}(-i, h)$ is completely within the region of \mathbf{Y}_2 . Given h , let \mathbf{X} only shift along y-axis. Then we have

$$(2.6) \quad \begin{bmatrix} \text{vec}(\mathbf{Z}(n_1, h))_{\mathbf{X}}^{\text{T}} \\ \text{vec}(\mathbf{Z}(n_1 + 1, h))_{\mathbf{X}}^{\text{T}} \\ \vdots \\ \text{vec}(\mathbf{Z}(k_1, h))_{\mathbf{X}}^{\text{T}} \end{bmatrix} \text{vec}(\mathbf{X}) + \begin{bmatrix} \text{vec}(\mathbf{Z}(k_1, -h))_{\mathbf{X}}^{\text{T}} \\ \text{vec}(\mathbf{Z}(k_1 - 1, -h))_{\mathbf{X}}^{\text{T}} \\ \vdots \\ \text{vec}(\mathbf{Z}(n_1, -h))_{\mathbf{X}}^{\text{T}} \end{bmatrix} \text{vec}(\mathbf{X}) = \mathbf{R}_1,$$

where $\text{vec}(\mathbf{Z}(i, h))_{\mathbf{X}}$ are those elements constrained in the region of \mathbf{X} . \mathbf{R}_1 is determined by $\mathbf{R}_{i, h}$ and \mathbf{Y} , where $i = n_1, \dots, k_1$, and $h = 0, \dots, n_2 + k_2 - 1$. Sliding \mathbf{X} in the region of \mathbf{Y}_2 yields a total of $(k_1 - n_1 + 1)(n_2 + k_2)$ different linear combinations of \mathbf{X} .

Secondly, we assume that $\mathbf{X}(-i, -h)$ overlaps with \mathbf{Y}_1 . Given i , \mathbf{X} is shifted along x-axis. Similarly, we have

$$(2.7) \quad \begin{bmatrix} \text{vec}(\mathbf{Z}(i, n_2))_{\mathbf{X}}^{\text{T}} \\ \text{vec}(\mathbf{Z}(i, n_2 + 1))_{\mathbf{X}}^{\text{T}} \\ \vdots \\ \text{vec}(\mathbf{Z}(i, k_2))_{\mathbf{X}}^{\text{T}} \end{bmatrix} \text{vec}(\mathbf{X}) + \begin{bmatrix} \text{vec}(\mathbf{Z}(-i, -n_2))_{\mathbf{X}}^{\text{T}} \\ \text{vec}(\mathbf{Z}(-i, -n_2 - 1))_{\mathbf{X}}^{\text{T}} \\ \vdots \\ \text{vec}(\mathbf{Z}(-i, -k_2))_{\mathbf{X}}^{\text{T}} \end{bmatrix} \text{vec}(\mathbf{X}) = \mathbf{R}_2,$$

where $-n_1 + 1 \leq i \leq n_1 - 1$, or \mathbf{X} is completely in the region of \mathbf{Y}_2 . As a result, the total number of linear combinations of $\text{vec}(\mathbf{X})$ in the second situation is $(k_2 - n_2 + 1)(2n_1 - 1)$.

To conclude, by combining equations (2.6) and (2.7) together, we obtain the following equations:

$$(2.8) \quad \mathbf{M} \text{vec}(\mathbf{X}) = \mathbf{R}_3.$$

Here, $\mathbf{M} \in \mathbb{R}^{((k_1 - n_1 + 1)(n_2 + k_2) + (k_2 - n_2 + 1)(2n_1 - 1)) \times n_1 n_2}$ represents combinations of all the matrices on the left side of the equations. Meanwhile, \mathbf{R}_3 is the vector stacked by the vectors on the right side of the equations.

It is worth noticing that, due to symmetry, at most half of $(k_1 - n_1 + 1)(n_2 + k_2) + (k_2 - n_2 + 1)(2n_1 - 1)$ equations will repeat. Since $\mathbf{Y}_{i, h} \stackrel{i.i.d}{\sim} \mathcal{N}(\mu, \sigma^2)$, $\sigma > 0$, if $(k_1 - n_1 + 1)(n_2 + k_2) + (k_2 - n_2 + 1)(2n_1 - 1) \geq 2n_1 n_2$, then \mathbf{M} is full column

rank with probability 1. We only need to prove that $\text{rank}(\mathbf{M}) \geq n_1 n_2$ to obtain this conclusion above, because $\text{rank}(\mathbf{M}) \leq n_1 n_2$.

Due to symmetry, we can construct a sub-matrix $\mathbf{M}_1 \in \mathbb{R}^{n_1 n_2 \times n_1 n_2}$ from \mathbf{M} where no two rows are the same. This is because $(k_1 - n_1 + 1)(n_2 + k_2) + (k_2 - n_2 + 1)(2n_1 - 1) \geq 2n_1 n_2$. By picking one row from each pair of equivalent rows, we can construct a sub-matrix \mathbf{M}_1 with a number of rows greater than $n_1 n_2$.

Because the determinant of \mathbf{M}_1 , denoted by $|\mathbf{M}_1|$, is a multivariate polynomial with variables $\mathbf{Y}_{i,h} \stackrel{i.i.d.}{\sim} \mathcal{N}(\mu, \sigma^2)$, the set of roots of $|\mathbf{M}_1|$ is defined as \mathbf{T} . Without loss of generality, we assume that there are d independent variables Y_1, Y_2, \dots, Y_d in \mathbf{M}_1 .

Using Lemma 4.1 in [36], which states that the roots of the finite real multivariate polynomial in d variables have a measure of zero in \mathbb{R}^d , we can conclude that \mathbf{T} has a measure of 0 in \mathbb{R}^d . Define the probability density function of each random variable Y_i as $\rho(Y_i)$, then the probability that

$$\begin{aligned} \mathbb{P}((Y_1, Y_2, \dots, Y_d) \in \mathbf{T}) &= \int_{(Y_1, Y_2, \dots, Y_d) \in \mathbf{T}} \rho(Y_1) \rho(Y_2) \cdots \rho(Y_d) dY_1 dY_2 \cdots dY_d \\ &\leq \int_{(Y_1, Y_2, \dots, Y_d) \in \mathbf{T}} dY_1 dY_2 \cdots dY_d \\ &= 0. \end{aligned}$$

The probability that $|\mathbf{M}_1|$ is nonzero is 1, meaning that $\text{rank}(\mathbf{M}) \geq \text{rank}(\mathbf{M}_1) = n_1 n_2$. Therefore, $\text{rank}(\mathbf{M}) = n_1 n_2$, and the signal of interest \mathbf{X} can be uniquely determined. \square

Next, we will generalize the result into higher dimensions.

LEMMA 2.4. *Consider the d -dimensional problem described by,*

$$(2.9) \quad \begin{aligned} &\text{Find } \mathbf{Z} \\ &\text{s.t. } \mathbf{I} = |\mathcal{F}(\mathbf{Z})|^2 \\ \mathbf{Z}_{i_1, i_2, \dots, i_d} &= \begin{cases} \mathbf{X}_{i_1, i_2, \dots, i_d}, & (i_1, i_2, \dots, i_d) \in \Omega \\ \mathbf{Y}_{i_1, i_2, \dots, i_d}, & \text{otherwise} \end{cases}, \end{aligned}$$

where $\mathcal{F}(\cdot)$ is the d dimensional discrete Fourier transform, $\mathbf{I} \in \mathbb{R}^{(n_1+k_1) \times (n_2+k_2) \cdots \times (n_d+k_d)}$, $\mathbf{Z} \in \mathbb{R}^{(n_1+k_1) \times (n_2+k_2) \cdots \times (n_d+k_d)}$, $\mathbf{Y} \in \mathbb{R}^{(n_1+k_1) \times (n_2+k_2) \cdots \times (n_d+k_d)}$ is the known background with $\mathbf{Y}_{i_1, i_2, \dots, i_d} \stackrel{i.i.d.}{\sim} \mathcal{N}(\mu, \sigma^2)$ where $(i_1, i_2, \dots, i_d) \notin \Omega$, else $\mathbf{Y}_{i_1, i_2, \dots, i_d} = 0$. If

$$\prod_{i=1}^d (n_i + k_i) \geq 2 \prod_{i=1}^d n_i + \prod_{i=1}^d (2n_i - 1),$$

then the solution of (2.9) is unique. In particular, when $n_i \equiv n$ and $k_i \equiv k, i = 1, 2, \dots, d$, then $k \geq (2^{\frac{d+1}{d}} - 1)n$ is sufficient to guarantee the unique solution.

Proof of Lemma 2.4. The sketch of the proof is similar to that of Theorem 2.1. The only difference is in the method used to count the number of linear equations of $\text{vec}(\mathbf{X})$.

For (2.9), $\prod_{i=1}^d (n_i + k_i)$ equations of $\text{vec}(\mathbf{X})$ will be obtained from \mathbf{I} by using the Wiener-Khinchin theorem and the definition of the high dimensional circular auto-correlation function below

$$\mathbf{R}_{i_1, i_2, \dots, i_d} = \text{vec}(\mathbf{Z}(-i_1, -i_2, \dots, -i_d))^T \text{vec}(\mathbf{Z}), 0 \leq i_h \leq n_h + k_h, h = 1, \dots, d.$$

Then, we can find that there are $\prod_{i=1}^m (2n_i - 1)$ nonlinear equations of $\text{vec}(\mathbf{X})$ (see Fig.2 to consider 2-D as a special case). Thus, there are $\prod_{i=1}^d (n_i + k_i) - \prod_{i=1}^m (2n_i - 1)$ linear combinations of $\text{vec}(\mathbf{X})$. Considering the symmetry of the equations, there are at least $\lfloor \frac{\prod_{i=1}^d (n_i + k_i) - \prod_{i=1}^m (2n_i - 1)}{2} \rfloor$ different equations with probability 1. By utilizing the same ideas in the proof of Theorem 2.1, we can conclude the proof. \square

Remark 2.5. In Lemma 2.4, we have $m_i \geq 2 \cdot 2^{\frac{1}{d}} n_i, i = 1, 2, \dots, d$, which is an extra factor of 2 compared to the number of measurements required by the traditional Fourier PR to guarantee a unique solution, namely $m_i \geq 2^{\frac{1}{d}} n_i, i = 1, 2, \dots, d$ [31]. Although (2.9) requires more measurements, it can guarantee an exact unique solution. This property cannot be achieved by traditional Fourier PR through sampling alone.

2.2. Stability of the solution. In this subsection, we will demonstrate another advantage of model (2.1), namely its stability. This can be used to estimate the distance between the iterations and the ground truth in real experiments.

THEOREM 2.6. *For the model (2.1), we assume that the background information $\mathbf{Y}_{i,h} \stackrel{i.i.d.}{\sim} \mathcal{N}(\mu, \sigma^2)$, $m_i = n_i + k_i, i = 1, 2$, and $m_1 m_2 \geq 2n_1 n_2 + (2n_1 - 1)(2n_2 - 1)$. If \mathbf{Y} is given, then for any $\mathbf{X}_1 \in \mathbb{R}^{n_1 \times n_2}$ and $\mathbf{X}_2 \in \mathbb{R}^{n_1 \times n_2}$, we have*

$$\|\mathbf{X}_1 - \mathbf{X}_2\|_F \leq \frac{\delta_1 \delta_2}{m_1 m_2} \|\text{vec}(\mathbf{I}_1 - \mathbf{I}_2)\|_1.$$

Here δ_1 and δ_2 are the largest singular values of $(\mathbf{M}^T \mathbf{M})^{-1}$, and \mathbf{M} respectively.

Proof. As demonstrated in the proof of Theorem 2.1, \mathbf{M} is of full column rank with probability 1, then we have

$$\begin{aligned} \|\mathbf{X}_1 - \mathbf{X}_2\|_F &= \|\text{vec}(\mathbf{X}_1) - \text{vec}(\mathbf{X}_2)\|_2 \\ &= \|(\mathbf{M}^T \mathbf{M})^{-1} \mathbf{M}^T (\mathbf{R}_3^1 - \mathbf{R}_3^2)\|_2 \\ &\leq \|(\mathbf{M}^T \mathbf{M})^{-1}\|_2 \|\mathbf{M}^T\|_2 \|\mathbf{R}_3^1 - \mathbf{R}_3^2\|_2 \\ (2.10) \quad &\stackrel{(a)}{\leq} \frac{1}{m_1 m_2} \|(\mathbf{M}^T \mathbf{M})^{-1}\|_2 \|\mathbf{M}^T\|_2 \|\text{vec}(\mathbf{I}_1 - \mathbf{I}_2)\|_1, \end{aligned}$$

where (a) is derived by the Wiener-Khinchin Theorem. \square

Remark 2.7. Suppose for all \mathbf{X} are bounded by a constant C namely $\|\mathbf{X}\|_F \leq C$. We can also derive the upper bound

$$\|\text{vec}(\mathbf{I}_1 - \mathbf{I}_2)\|_1 \leq m_2 \|\mathbf{I}_1 - \mathbf{I}_2\|_1 \leq \sqrt{m_1 m_2} \|\mathbf{I}_1 - \mathbf{I}_2\|_F \leq 2C m_1^{\frac{3}{2}} m_2^2 \|\mathbf{X}_1 - \mathbf{X}_2\|_F,$$

where the second inequality is derived by the Cauchy-Schwartz inequality. The last

inequality is achieved by:

$$\begin{aligned}
\|\mathbf{I}_1 - \mathbf{I}_2\|_{\mathbb{F}}^2 &= \sum_{l=1}^{m_1} \sum_{h=1}^{m_2} (\mathbf{I}_{1,l,h} - \mathbf{I}_{2,l,h})^2 \\
&= \sum_{l=1}^{m_1} \sum_{h=1}^{m_2} (\sqrt{\mathbf{I}_{1,l,h}} + \sqrt{\mathbf{I}_{2,l,h}})^2 (\sqrt{\mathbf{I}_{1,l,h}} - \sqrt{\mathbf{I}_{2,l,h}})^2 \\
&\leq \sum_{l=1}^{m_1} \sum_{h=1}^{m_2} 2(\mathbf{I}_{1,l,h} + \mathbf{I}_{2,l,h}) (\sqrt{\mathbf{I}_{1,l,h}} - \sqrt{\mathbf{I}_{2,l,h}})^2 \\
&\stackrel{(a)}{\leq} 4C^2 m_1 m_2 \sum_{l=1}^{m_1} \sum_{h=1}^{m_2} (\sqrt{\mathbf{I}_{1,l,h}} - \sqrt{\mathbf{I}_{2,l,h}})^2 \\
&\stackrel{(b)}{\leq} 4C^2 m_1^2 m_2^2 \sum_{l=1}^{m_1} \sum_{h=1}^{m_2} (\mathbf{X}_{1,l,h} - \mathbf{X}_{2,l,h})^2,
\end{aligned}$$

where (a) is derived by the Parseval's theorem, and (b) is achieved by triangle inequality and Parseval's theorem.

2.3. Robustness of the solution. Next, we analyze the situation in which the known background information \mathbf{Y} has bias and the intensity-only measurements \mathbf{I} are corrupted by noise. Under these conditions, we estimate the solution \mathbf{X}^* by solving the least square problem:

$$(2.11) \quad \mathbf{X}^* \in \arg \min_{\mathbf{X} \in \mathbb{R}^{n_1 \times n_2}} \|\mathbf{M} \text{vec}(\mathbf{X}) - \tilde{\mathbf{R}}_3\|_2^2,$$

where $\tilde{\mathbf{R}}_3$ is the corruption of \mathbf{R}_3 . If \mathbf{M} has full column rank, then \mathbf{X}^* has the closed form:

$$\text{vec}(\mathbf{X}^*) = (\mathbf{M}^T \mathbf{M})^{-1} \mathbf{M}^T \tilde{\mathbf{R}}_3.$$

Next, we provide a bound for the distance between \mathbf{X}^* and the ground truth \mathbf{X} . Although we only consider the 2-D case, it can be generalized to higher-dimensional situations accordingly.

THEOREM 2.8. *For model (2.1), we assume that $\mathbf{Y}_{i,h} \stackrel{i.i.d}{\sim} \mathcal{N}(\mu, \sigma^2)$, $m_i = n_i + k_i$, $i = 1, 2$, and $m_1 m_2 \geq 2n_1 n_2 + (2n_1 - 1)(2n_2 - 1)$. $\tilde{\mathbf{I}}$ is the intensity-only measurements that are corrupted by bounded random noise $\boldsymbol{\varepsilon}_1$ such that $\max(|\boldsymbol{\varepsilon}_1|) \leq c_1$. The known background information $\tilde{\mathbf{Y}}$ also contains bounded random bias $\boldsymbol{\varepsilon}_2$ with $\max(|\boldsymbol{\varepsilon}_2|) \leq c_2$. With probability 1, the estimation \mathbf{X}^* calculated by (2.11) and the ground truth \mathbf{X} satisfy the following inequality:*

$$\|\mathbf{X}^* - \mathbf{X}\|_{\mathbb{F}} \leq \delta_1 \delta_2 \left(c_1 + c_2 \left(2\|\text{vec}(\tilde{\mathbf{Y}})\|_1 + c_2 m_1 m_2 \right) + \frac{\sqrt{C_2(c_2)\|\text{vec}(\tilde{\mathbf{I}})\|_1 + C_1(c_1, c_2)}}{m_1 m_2} \right),$$

where δ_1 and δ_2 are the largest singular values of $(\tilde{\mathbf{M}}^T \tilde{\mathbf{M}})^{-1}$, and $\tilde{\mathbf{M}}$ respectively. $\tilde{\mathbf{M}}$ is the corruption of \mathbf{M} . C_1 and C_2 are constants depending on c_1 and c_2 .

Proof. Utilizing the same techniques as in proving Theorem 2.1, we can demonstrate that $\tilde{\mathbf{M}}$ is also of full column rank with probability 1 when being corrupted by

bounded random noise ε_1 . Then we can have

$$\begin{aligned}
\|\mathbf{X}^* - \mathbf{X}\|_F &= \|\text{vec}(\mathbf{X}^*) - \text{vec}(\mathbf{X})\|_2 \\
&= \left\| (\tilde{\mathbf{M}}^T \tilde{\mathbf{M}})^{-1} \tilde{\mathbf{M}}^T \tilde{\mathbf{R}}_3 - \text{vec}(\mathbf{X}) \right\|_2 \\
&\leq \left\| (\tilde{\mathbf{M}}^T \tilde{\mathbf{M}})^{-1} \right\|_2 \left\| \tilde{\mathbf{M}}^T (\tilde{\mathbf{R}}_3 - \tilde{\mathbf{M}} \text{vec}(\mathbf{X})) \right\|_2 \\
&\stackrel{(a)}{=} \left\| (\tilde{\mathbf{M}}^T \tilde{\mathbf{M}})^{-1} \right\|_2 \left\| \tilde{\mathbf{M}}^T (\mathbf{M} \text{vec}(\mathbf{X}) - \mathbf{R}_3 + \tilde{\mathbf{R}}_3 - \tilde{\mathbf{M}} \text{vec}(\mathbf{X})) \right\|_2 \\
(2.12) \quad &\leq \left\| (\tilde{\mathbf{M}}^T \tilde{\mathbf{M}})^{-1} \right\|_2 \left\| \tilde{\mathbf{M}}^T \right\|_2 \left(\left\| \mathbf{M} - \tilde{\mathbf{M}} \right\|_2 \|\text{vec}(\mathbf{X})\|_2 + \left\| \tilde{\mathbf{R}}_3 - \mathbf{R}_3 \right\|_2 \right),
\end{aligned}$$

where (a) is derived by the (2.8), and $\tilde{\mathbf{R}}_3$ is the corruption of \mathbf{R}_3 . Next, we will divide (2.12) into three parts to analyze.

For $\left\| \mathbf{M} - \tilde{\mathbf{M}} \right\|_2$, the relationship below can be held

$$\begin{aligned}
\left\| \mathbf{M} - \tilde{\mathbf{M}} \right\|_2 &\leq \left\| \mathbf{M} - \tilde{\mathbf{M}} \right\|_F \\
(2.13) \quad &\leq 2\sqrt{n_1 n_2 m_1 m_2} c_2.
\end{aligned}$$

Specifically, define $\mathbf{D} := \mathbf{M} - \tilde{\mathbf{M}}$, where the total number of elements of \mathbf{D} is less than $n_1 n_2 m_1 m_2$. Then based on the structure of \mathbf{M} and $\tilde{\mathbf{M}}$, we have

$$|\mathbf{D}_{i,k}| = |\mathbf{M}_{i,k} - \tilde{\mathbf{M}}_{i,k}| \leq 2c_2,$$

where the inequality is derived by the Cauchy-Schwarz inequality.

Next, for $\|\text{vec}(\mathbf{X})\|_2$, we can obtain the following relationship using Parseval's theorem and the triangle inequality:

$$\begin{aligned}
\|\text{vec}(\mathbf{X})\|_2^2 &= \frac{1}{m_1 m_2} \sum_{i=1}^{m_1} \sum_{k=1}^{m_2} (\tilde{\mathbf{I}}_{i,k} - \varepsilon_{1,i,k}) \\
(2.14) \quad &\leq \frac{1}{m_1 m_2} \left\| \text{vec}(\tilde{\mathbf{I}}) \right\|_1 + c_1.
\end{aligned}$$

Finally, for $\left\| \tilde{\mathbf{R}}_3 - \mathbf{R}_3 \right\|_2$, it can be divided into two parts based on the structures of \mathbf{R}_3 : auto-correlation \mathbf{R} and multiplications of background information. With a similar idea, by using the Parseval's theorem, Wiener-Khinchin theorem and Cauchy-Schwarz inequality, relationship can be held below

$$(2.15) \quad \left\| \tilde{\mathbf{R}}_3 - \mathbf{R}_3 \right\|_2 \leq m_1 m_2 \left(c_1 + 2c_2 \|\text{vec}(\tilde{\mathbf{Y}})\|_1 + c_2^2 m_1 m_2 \right).$$

Accordingly, define $\mathbf{D} := \tilde{\mathbf{R}}_3 - \mathbf{R}_3$. For each element D_i , it can be divided into two parts namely the difference of the auto-correlation $\tilde{\mathbf{R}}_{i,k} - \mathbf{R}_{i,k}$ and the difference of the multiplications of background information $\sum_{i_1, k_1, i_2, k_2} (\tilde{\mathbf{Y}}_{i_1, k_1} \tilde{\mathbf{Y}}_{i_2, k_2} - \mathbf{Y}_{i_1, k_1} \mathbf{Y}_{i_2, k_2})$.

Because

$$\begin{aligned}
& \left| \sum_{i_1, k_1, i_2, k_2} (\tilde{\mathbf{Y}}_{i_1, k_1} \tilde{\mathbf{Y}}_{i_2, k_2} - \mathbf{Y}_{i_1, k_1} \mathbf{Y}_{i_2, k_2}) \right| \\
& \leq \sum_{i_1, k_1, i_2, k_2} \left| \tilde{\mathbf{Y}}_{i_1, k_1} \tilde{\mathbf{Y}}_{i_2, k_2} - (\tilde{\mathbf{Y}}_{i_1, k_1} - \varepsilon_{2_{i_1, k_1}})(\tilde{\mathbf{Y}}_{i_2, k_2} - \varepsilon_{2_{i_2, k_2}}) \right| \\
& \leq \sum_{i_1, k_1, i_2, k_2} \left| \tilde{\mathbf{Y}}_{i_1, k_1} \varepsilon_{2_{i_2, k_2}} + \tilde{\mathbf{Y}}_{i_2, k_2} \varepsilon_{2_{i_1, k_1}} - \varepsilon_{2_{i_1, k_1}} \varepsilon_{2_{i_2, k_2}} \right| \\
& \leq \sum_{i_1, k_1, i_2, k_2} c_2 \left| \tilde{\mathbf{Y}}_{i_1, k_1} \right| + c_2 \left| \tilde{\mathbf{Y}}_{i_2, k_2} \right| + c_2^2 \\
& \leq 2c_2 \|\text{vec}(\tilde{\mathbf{Y}})\|_1 + c_2^2 m_1 m_2.
\end{aligned}$$

Then, we have

$$\begin{aligned}
\|\mathbf{D}\|_2 & \leq \|\text{vec}(\tilde{\mathbf{R}} - \mathbf{R})\|_1 + m_1 m_2 \left(2c_2 \|\text{vec}(\tilde{\mathbf{Y}})\|_1 + c_2^2 m_1 m_2 \right) \\
& \leq \sqrt{m_1 m_2 \|\tilde{\mathbf{R}} - \mathbf{R}\|_F^2} + m_1 m_2 \left(2c_2 \|\text{vec}(\tilde{\mathbf{Y}})\|_1 + c_2^2 m_1 m_2 \right) \\
& \leq \|\tilde{\mathbf{I}} - \mathbf{I}\|_F + m_1 m_2 \left(2c_2 \|\text{vec}(\tilde{\mathbf{Y}})\|_1 + c_2^2 m_1 m_2 \right) \\
& \leq \|\varepsilon_1\|_F + m_1 m_2 \left(2c_2 \|\text{vec}(\tilde{\mathbf{Y}})\|_1 + c_2^2 m_1 m_2 \right).
\end{aligned}$$

Thus, combining (2.13), (2.14), and (2.15), we can finish the conclusion. \square

Remark 2.9. In Theorem 2.8, the right hand side of the inequality is composed of three parts. The first part is the influence caused by measurement noise c_1 . The second part is the influence caused by the bias of the background information $C_2(c_2)\|\text{vec}(\tilde{\mathbf{I}})\|_1$, and $c_2 \left(2\|\text{vec}(\tilde{\mathbf{Y}})\|_1 + c_2 m_1 m_2 \right)$. The third part is the coupling between the measurement error and bias of the background information namely $C_1(c_1, c_2)$. When $c_1 = 0$, that is to say there is no measurement noise, then we have

$$\|\mathbf{X}^* - \mathbf{X}\|_F \leq \delta_1 \delta_2 \left(c_2 \left(2\|\text{vec}(\tilde{\mathbf{Y}})\|_1 + c_2 m_1 m_2 \right) + \frac{\sqrt{C_2(c_2)\|\text{vec}(\tilde{\mathbf{I}})\|_1}}{m_1 m_2} \right).$$

When $c_2 = 0$ namely there is no bias of the background information, we can achieve the relationship below

$$\|\mathbf{X}^* - \mathbf{X}\|_F \leq c_1 \delta_1 \delta_2.$$

3. Methods to find the ground truth. In this section, we assume that the length of the background information is sufficient to ensure that (3.1) has a unique solution. We will introduce two methods based on the Douglas-Rachford method to find the ground truth. These methods include the convex and non-convex types. For simplicity, we will only discuss the 1-D formulation of the problem, but the situation in higher dimensions can be generalized.

3.1. Background Douglas Rachford method. Denoting $\mathbf{z} = [z_1, \dots, z_{n+k}]^T$, the 1-D Fourier PR model with background information can be formulated as below

$$(3.1) \quad \begin{aligned} & \text{Find } \mathbf{z} \\ & \text{s.t. } |\mathbf{F}_i^H \mathbf{z}|^2 = b_i, i = 1, \dots, m \\ & \quad z_{n+l} = y_l, l = 1, \dots, k. \end{aligned}$$

Define set \mathbf{A} and \mathbf{B} as below:

$$\begin{aligned} \mathbf{A} & := \left\{ \mathbf{z} \in \mathbb{R}^{n+k} : |\mathbf{F}^H \mathbf{z}| = \mathbf{b}^{\frac{1}{2}} \right\} \\ \mathbf{B} & := \left\{ \mathbf{z} \in \mathbb{R}^{n+k} : z_{n+i} = y_i, i = 1, \dots, k \right\}. \end{aligned}$$

\mathbf{A} and \mathbf{B} are closed sets, however \mathbf{A} is not convex. $\mathbf{A} \cap \mathbf{B}$ is actually the set of solution in (3.1). The projection of $\mathbf{z} \in \mathbb{R}^{n+k}$ onto a closed set \mathbf{C} is defined as

$$\mathbb{P}_{\mathbf{C}}(\mathbf{z}) := \arg \min_{\mathbf{x} \in \mathbf{C}} \|\mathbf{x} - \mathbf{z}\|_2^2.$$

Notice that, when $z_i = 0$, $i \in \{1, \dots, n+k\}$, $\mathbb{P}_{\mathbf{C}}(\mathbf{z})$ may be not unique. In the previous work, [1] reformulated (3.1) as a constrained optimization problem below

$$(3.2) \quad \begin{aligned} \underset{\mathbf{z} \in \mathbb{R}^{n+k}}{\text{minimize}} \quad f(\mathbf{z}) & = \frac{1}{2(n+k)} \sum_{i=1}^{n+k} \left(|\mathbf{F}_i^H \mathbf{z}| - b_i^{\frac{1}{2}} \right)^2 \\ \text{s.t.} \quad \mathbf{z} & \in \mathbf{B} \quad . \end{aligned}$$

Then, the projected gradient descent (PGD) method is utilized to search for the ground truth. The main procedure in the p th step is:

$$\begin{cases} \tilde{\mathbf{z}}^p = \mathbf{z}^{p-1} - \lambda \partial f(\mathbf{z}^{p-1}) \\ \mathbf{z}^p = \mathbb{P}_{\mathbf{B}}(\tilde{\mathbf{z}}^p) \end{cases},$$

where $\partial f(\mathbf{z}^{p-1}) = \mathbf{z}^{p-1} - \mathbb{P}_{\mathbf{A}}(\mathbf{z}^{p-1})$, and λ is the learning rate. When λ is set to 1, it ensures that $f(\mathbf{z}^p) \leq f(\mathbf{z}^{p-1})$. In this case, the PGD method is equivalent to the alternating minimization method [11]. Although [1] provides numerous tests to demonstrate the advantages of the PGD method. However, it is prone to stagnation and demands a large number of background information, nearly $k \geq 6n$, to achieve a higher recovery rate.

In many literatures, the traditional Fourier PR problem has been solved using the Douglas Rachford (DR) method [11], which has demonstrated better performance than the PGD method. In this work, we apply a reflection-based method called background Douglas-Rachford (BDR) method to solve (3.1). See Fig.3 for an example. The length of the background information is 10. Both methods have a common initialization of $(-0.82, 1.26, 0.56)$. We observe that the PGD method easily stagnates, but the BDR method can overcome such traps and converge to the ground truth. The details of the BDR method are shown in Algorithm 3.1.

As discussed above, the most significant difference between the PGD and BDR methods is the general step in Algorithm 3.1. For the PGD method, this involves creating a sequence $\{\mathbf{z}^p\}$ by applying alternative projection to approximate $\mathbf{A} \cap \mathbf{B}$:

$$\mathbf{z}^p = \mathbb{P}_{\mathbf{B}} \mathbb{P}_{\mathbf{A}}(\mathbf{z}^{p-1}).$$

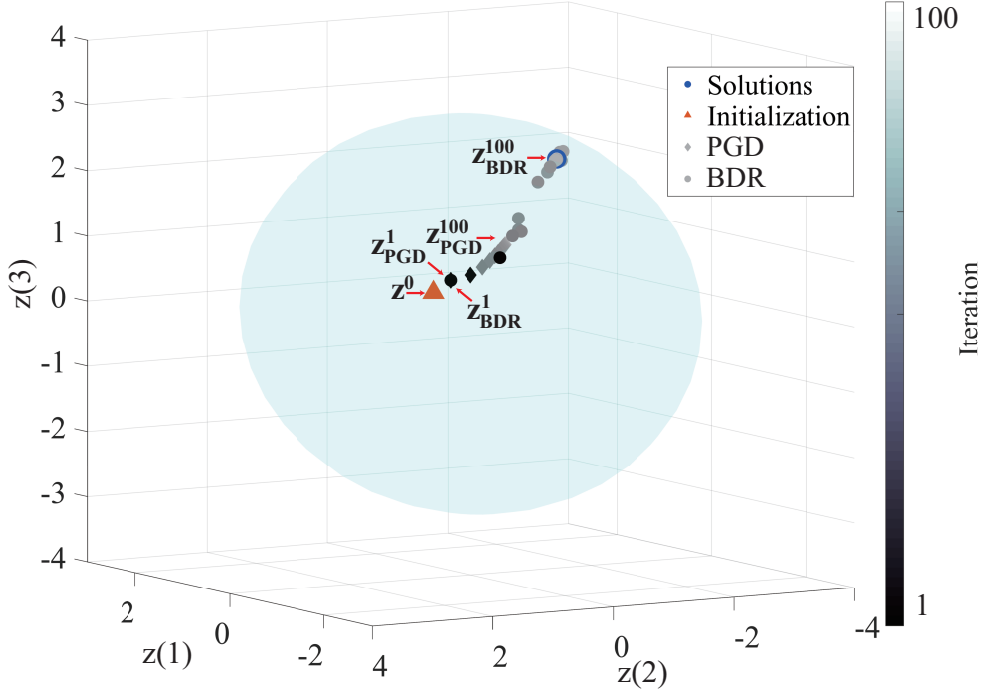


Fig. 3: The comparison between Projected Gradient Descent (PGD) method and the background Douglas-Rachford (BDR) method, both of which aim to find the ground truth value of $(-1.52, -0.24, 2.61)$. The background information has a length of 10, and both methods are initialized with the same values of $(-0.82, 1.26, 0.56)$. While PGD stagnates easily, the BDR method can escape the trap and converge to the ground truth.

Because $\mathbb{P}_B \mathbb{P}_A$ is not a strict contraction operator, the PGD method is liable to converge to a fixed point which is usually not the ground truth. For the BDR method, it defines an operator $\mathbb{T}(\cdot)$, and

$$(3.3) \quad \mathbf{z}^p = \mathbb{T}(\mathbf{z}^{p-1}) = \frac{1}{2}(\mathbb{R}_B \mathbb{R}_A + \mathbb{I})(\mathbf{z}^{p-1}),$$

where $\mathbb{R}_A(\cdot)$ and $\mathbb{R}_B(\cdot)$ are the reflectors namely

$$\mathbb{R}_A(\cdot) = 2\mathbb{P}_A(\cdot) - \mathbb{I}(\cdot), \quad \mathbb{R}_B(\cdot) = 2\mathbb{P}_B(\cdot) - \mathbb{I}(\cdot), \quad \text{where } \mathbb{I}(\cdot) \text{ is the unit projector.}$$

By reformulating (3.3) as below

$$\begin{aligned} \mathbf{z}^p &= \frac{1}{2}((2\mathbb{P}_B - \mathbb{I})(2\mathbb{P}_A - \mathbb{I}) + \mathbb{I})(\mathbf{z}^{p-1}) \\ &= (\mathbb{P}_B(2\mathbb{P}_A - \mathbb{I}) + (\mathbb{I} - \mathbb{P}_A))(\mathbf{z}^{p-1}) \\ &\stackrel{(a)}{=} \mathbf{1}_n \odot (2\mathbb{P}_A(\mathbf{z}^{p-1}) - \mathbf{z}^{p-1}) + (\mathbf{z}^{p-1} - \mathbb{P}_A(\mathbf{z}^{p-1})) + \tilde{\mathbf{y}} \\ &= \mathbf{1}_n \odot \mathbb{P}_A(\mathbf{z}^{p-1}) + (\mathbf{1} - \mathbf{1}_n) \odot (\mathbf{z}^{p-1} - \mathbb{P}_A(\mathbf{z}^{p-1}) + \tilde{\mathbf{y}}), \end{aligned}$$

Algorithm 3.1 The Background Douglas Rachford method

Input: $\{\mathbf{b}, \mathbf{y}, \varepsilon, T\}$ \mathbf{b} : the intensity only Fourier measurement. \mathbf{y} : the background information. ε : the allowed error bound. T : the maximum allowed iteration.**Output:** $\bar{\mathbf{x}}$: an estimation of the real signal \mathbf{x} .

Initialization :1: $\mathbf{z}^0 = \mathbb{P}_{\mathbf{B}}(\frac{1}{n+k}\mathbf{F} \cdot \mathbf{b}^{\frac{1}{2}})$, $\mathbf{B} = \{\mathbf{z} : z_{n+i} = y_i, i = 1, \dots, k\}$.2: $p = 1$.**General step**1: $\tilde{\mathbf{z}}^{p-1} = \mathbb{P}_{\mathbf{A}}(\mathbf{z}^{p-1})$, where $\mathbf{A} = \{\mathbf{z} : |\mathbf{F}^H \mathbf{z}| = \mathbf{b}^{\frac{1}{2}}\}$ 2: $z_t^p = \tilde{z}_t^{p-1}, t = 1, \dots, n$, $z_{n+t}^p = z_{n+t}^{p-1} - \tilde{z}_{n+t}^{p-1} + y_t, t = 1, \dots, k$.3: **if** $\|\mathbf{z}^p - \mathbf{z}^{p-1}\|_2 \leq \varepsilon$ **or** $p = T + 1$ **then**4: $\bar{\mathbf{z}} = \mathbf{z}^p$.5: $\bar{\mathbf{x}} = [\bar{z}_1, \bar{z}_2, \dots, \bar{z}_n]^T$.

6: Break.

7: **end if**8: $p = p + 1$

where (a) is deduced from the definition of $\mathbb{P}_{\mathbf{B}}(\cdot)$, where $\mathbf{1}_n \in \mathbb{R}^{n+k}$ is a vector whose first n elements are 1, and the rest are 0, and $\tilde{\mathbf{y}} = [\mathbf{0}; \mathbf{y}] \in \mathbb{R}^{n+k}$. This allows us to obtain the main step in Algorithm 3.1.

One advantage of Algorithm 3.1 is that if we can find the fixed points, we can derive the ground truth from them. This is proven by the following theorem.

THEOREM 3.1. *If Algorithm 3.1 converges to $\bar{\mathbf{z}}$, which is one of the fixed points of \mathbb{T} , then $\mathbb{P}_{\mathbf{B}}\bar{\mathbf{z}}$ is a solution to (3.1).*

Proof of Theorem 3.1. If $\bar{\mathbf{z}}$ is one of the stationary points namely $\bar{\mathbf{z}} = \mathbb{T}(\bar{\mathbf{z}})$. Recalling Algorithm 3.1, we have

$$\begin{aligned} \tilde{\bar{z}}_t &= \mathbb{T}(\bar{\mathbf{z}})_t = \bar{z}_t, \quad 1 \leq t \leq n \\ \tilde{\bar{z}}_t &= y_{t-n}, \quad n+1 \leq t \leq n+k. \end{aligned}$$

Because $|\mathbf{F}^H \tilde{\bar{\mathbf{z}}}|^2 = \mathbf{b}$, $\tilde{\bar{\mathbf{z}}} = \mathbb{P}_{\mathbf{B}}(\tilde{\bar{\mathbf{z}}})$ is one of the solutions of (3.1). In particular, if \mathbf{y} is sufficient, Theorem 2.1 guarantees that the solution is uniquely determined. \square

Next, we will prove the local R-linear convergence of Algorithm 3.1. Before proceeding, we will make some assumptions.

ASSUMPTION 3.2.

1. $m \geq 2(n+k) - 1$ namely we have oversampled the Fourier amplitude \mathbf{b} with over $2(n+k) - 1$ measurements.
2. $\mathbf{x} \neq \mathbf{0}$ and the z -transform of the ground truth $\mathbf{z} = [\mathbf{x}; \mathbf{y}]$ has no zeros in the reciprocal pairs.

The z -transform of a vector \mathbf{x} is denoted by $X(z)$. There are no zeros in the reciprocal pairs means that if $X(z_1) = 0$, then $X(1/\bar{z}_1) \neq 0$. By changing the values of

background information, the second assumption can be satisfied.

THEOREM 3.3. *For model (3.1), define*

$$\begin{aligned}\mathbf{A} &:= \{\mathbf{z} \in \mathbb{R}^{n+k} : |\mathbf{F}^H \mathbf{z}| = \mathbf{b}^{\frac{1}{2}}, \mathbf{b} \in \mathbb{R}^m\} \\ \mathbf{B} &:= \{\mathbf{z} \in \mathbb{R}^{n+k} : z_{n+i} = y_i, i = 1, \dots, k\}.\end{aligned}$$

$\mathbf{F} \in \mathbb{C}^{n \times m}$ is an oversampling Fourier matrix, where $m \geq 2(n+k) - 1$. Suppose there exists $\delta > 0$ such that the initialization \mathbf{z}^0 is sufficient close to the ground truth $\mathbf{z} \in \mathbf{A} \cap \mathbf{B}$, specially

$$\|\mathbf{z}^0 - \mathbf{z}\|_2 \leq \frac{\delta}{2},$$

then the sequence $\{\mathbf{z}^p\}$ generated by Algorithm 3.1 converges to \mathbf{z} with R-linear rate, i.e., there exists a constant $\gamma \in [0, 1)$ such that

$$\|\mathbf{z}^p - \mathbf{z}\|_2 \leq \frac{\|\mathbf{z}^0 - \mathbf{z}\|_2 (1 + \gamma)}{1 - \gamma} \gamma^p.$$

The sketch of the proof is to establish that \mathbf{A} and \mathbf{B} are super-regular at $\mathbf{z} \in \mathbf{A} \cap \mathbf{B}$, and the system $\{\mathbf{A}, \mathbf{B}\}$ is strongly regular at \mathbf{z} . The results can then be obtained using the theories presented in [37]. For details, please refer to Appendix A.

In this subsection, we develop the BDR method to solve (3.1). Although it has been proven that the BDR method exhibits local R-linear convergence, the theoretical results presented above are not optimal. First, the convergence of BDR is local which requires the initialization to be close to the ground truth. This is challenge to achieve in practice. Second, there is a difference between theories and applications. While the BDR method performs well in numerical tests when $m = n + k$, theories demand $m \geq 2(n+k) - 1$. Additionally, calculating the operator $\mathbb{P}_{\mathbf{A}}$ is challenging when $m \geq 2(n+k) - 1$ in the BDR method.

As a result, in the next subsection, we introduce a convex variant of the BDR method called CBDR method. This method guarantees a global convergence rate and is easier to apply.

3.2. Convex Background Douglas Rachford method. In this subsection, we reformulate (3.1) and try to solve the problem below,

$$(3.4) \quad \begin{aligned} &\text{Find } \mathbf{z} \\ &\text{s.t. } |\mathbf{F}_i^H \mathbf{z}|^2 \leq b_i, i = 1, \dots, m \\ &\quad z_{n+l} = y_l, l = 1, \dots, k. \end{aligned}$$

(3.4) is actually a convex problem. Specifically if any \mathbf{x}^1 and \mathbf{x}^2 are the solutions of (3.4), for $0 \leq \lambda \leq 1$, we have $\lambda x_{n+l}^1 + (1 - \lambda)x_{n+l}^2 = y_l, l = 1, \dots, k$, and

$$|\mathbf{F}_i^H (\lambda \mathbf{x}^2 + (1 - \lambda)\mathbf{x}^1)|^2 \leq (\lambda |\mathbf{F}_i^H \mathbf{x}^1| + (1 - \lambda) |\mathbf{F}_i^H \mathbf{x}^2|)^2 \leq b_i.$$

If we can demonstrate that (3.1) and (3.4) have the same solution for a sufficiently large length of background information k , we can obtain the ground truth of the non-convex problem (3.1) by solving the convex problem (3.4). then a batch of efficient algorithms with theoretical convergence guarantees can be applied. Theorem 3.4 can guarantee this property.

THEOREM 3.4. *Assuming $k > \max \left\{ \frac{n}{1-\delta}, \frac{8c\|\mathbf{x}\|_2}{\delta\sqrt{\eta}}, \frac{16c(\sqrt{\delta}+2)^2 \log(\frac{1}{\eta})}{\delta^2}, c(n, \delta) \right\}$, then the probability of the solution being the same for both (3.1) and (3.4) is no less than $1 - \eta$. Here $\delta \in (0, 1)$, c is a constant and $c(n, \delta)$ is a constant that depends on n and δ . For details on $c(n, \delta)$, refer to (B.5).*

Remark 3.5. In [38], it is proven that the natural least squares formulation for affine phase retrieval is strongly convex on the entire space, provided that the measurements are complex Gaussian random vectors and the number of measurements is sufficient.

However, the main idea to convexify the problem in this subsection is to reformulate $\mathbf{A} := \left\{ \mathbf{z} \in \mathbb{R}^{n+k} : |\mathbf{F}^H \mathbf{z}| = \mathbf{b}^{\frac{1}{2}} \right\}$ to be convex while ensuring that $\mathbf{A} \cap \mathbf{B}$ still belongs to the solutions of (3.1). To achieve this, we redefine \mathbf{A} as follows:

$$\mathbf{A} := \left\{ \mathbf{z} \in \mathbb{R}^{n+k} : |\mathbf{F}_i^H \mathbf{z}| \leq b_i^{\frac{1}{2}}, i = 1, \dots, n+k \right\}.$$

To prove Theorem 3.4, a matrix \mathbf{L} is constructed. Each column of this matrix is a circular shift of \mathbf{z} , which is one of the solutions of (3.1).

$$\mathbf{L} = \begin{pmatrix} z_1 & z_2 & \cdots & z_n & z_{n+1} & \cdots & z_{n+k-1} & z_{n+k} \\ z_2 & z_3 & \cdots & z_{n+1} & z_{n+2} & \cdots & z_{n+k} & z_1 \\ \vdots & \vdots & \cdots & \vdots & \vdots & \ddots & \vdots & \vdots \\ z_n & z_{n+1} & \cdots & z_{2n} & z_{2n+1} & \cdots & z_{n-2} & z_{n-1} \\ z_{n+1} & z_{n+2} & \cdots & z_{2n+1} & z_{2n+2} & \cdots & z_{n-1} & z_n \\ \vdots & \vdots & \cdots & \vdots & \vdots & \ddots & \vdots & \vdots \\ z_{n+k-1} & z_{n+k} & \cdots & z_{n-2} & z_{n-1} & \cdots & z_{n+k-3} & z_{n+k-2} \\ z_{n+k} & z_1 & \cdots & z_{n-1} & z_n & \cdots & z_{n+k-2} & z_{n+k-1} \end{pmatrix}.$$

Note that $\mathbf{z} = [\mathbf{x}, \mathbf{y}]$, where $\mathbf{x} := [z_1, z_2, \dots, z_n]$ and $\mathbf{y} := [z_{n+1}, z_{n+2}, \dots, z_{n+k}]$, and each element of \mathbf{y} satisfies a normal distribution $\mathcal{N}(0, 1)$ independently. The theory below proves that \mathbf{L} is non-singular with probability 1.

LEMMA 3.6. *Assume $\mathbf{x} \in \mathbb{R}^n$ is given, as if $k \geq 1$, then $\mathbf{L} \in \mathbb{R}^{(n+k) \times (n+k)}$ is non-singular with probability 1.*

Proof. To prove Lemma 3.6, we can use the similar algebraic tools used in the proof of Theorem 2.1 to show that the set of vectors \mathbf{y} which satisfy $|\mathbf{L}| = 0$ has measure 0 in \mathbb{R}^k . \square

If \mathbf{L} is non-singular, its columns can span the \mathbb{R}^{n+k} space. Let us define

$$\mathbf{e}_1 = [1; 0; \dots, 0].$$

We can find that $\mathbf{L}\mathbf{e}_1 := \mathbf{z}$, which is one of the solutions of (3.4). If there are other solutions of (3.4) except \mathbf{z} , then $\exists \mathbf{h} \in \mathbb{R}^{n+k}$ and $\mathbf{h} \neq \mathbf{0}$ such that the sub-matrix \mathbf{L}_1 of \mathbf{L} satisfies $\mathbf{L}_1 \mathbf{h} = \mathbf{0}$, where

$$\mathbf{L}_1 := \begin{pmatrix} z_{n+1} & z_{n+2} & \cdots & z_{2n+1} & z_{2n+2} & \cdots & z_{n-1} & z_n \\ \vdots & \vdots & \cdots & \vdots & \vdots & \ddots & \vdots & \vdots \\ z_{n+k-1} & z_{n+k} & \cdots & z_{n-2} & z_{n-1} & \cdots & z_{n+k-3} & z_{n+k-2} \\ z_{n+k} & z_1 & \cdots & z_{n-1} & z_n & \cdots & z_{n+k-2} & z_{n+k-1} \end{pmatrix},$$

where \mathbf{L}_1 is a partial circulant measurement matrix.

The vector \mathbf{h} mentioned earlier exists inherently because $\text{Rank}(\mathbf{L}_1) \leq k$, which implies that $\text{Ker}(\mathbf{L}_1) \geq n$. Therefore, a space in \mathbb{R}^{n+k} exists, with dimension larger than n , that is a subset of $\text{Ker}(\mathbf{L}_1)$.

On the other hand, if $\mathbf{L}\mathbf{h}$ is a solution of (3.4), then $|\mathbf{F}_i^H \mathbf{L}\mathbf{h}|^2 \leq b_i, i = 1, \dots, n+k$. Note that \mathbf{L} is a circulant matrix, so we have:

$$\mathbf{F}\mathbf{L}\mathbf{h} = (\mathbf{F}\mathbf{z}) \odot (\mathbf{F}\mathbf{h}),$$

where \odot is the Hadamard product, and \mathbf{F} is the Fourier matrix with the i th row being \mathbf{F}_i^H . Using the property of Fourier transform, we have:

$$|\mathbf{F}_i^H \mathbf{L}\mathbf{h}|^2 = |\mathbf{F}_i^H \mathbf{z}|^2 |\mathbf{F}_i^H \mathbf{h}|^2 \leq b_i, i = 1, \dots, n+k.$$

Since $|\mathbf{F}_i^H \mathbf{z}|^2 = b_i$, we have $|\mathbf{F}_i^H \mathbf{h}|^2 \leq 1, i = 1, \dots, n+k$.

Combining the two situations above, we can conclude that if the sets \mathbf{C}_1 and \mathbf{C}_2 satisfy $\mathbf{C}_1 \cap \mathbf{C}_2 = \{\mathbf{0}\}$, then only one point \mathbf{z} satisfies the constraint in (3.4). The sets are defined as follows:

$$\begin{aligned} \mathbf{C}_1 &:= \{\mathbf{h} | \mathbf{L}_1 \mathbf{h} = \mathbf{0}\}, \\ \mathbf{C}_2 &:= \{\mathbf{h} | |\mathbf{F}_i^H \mathbf{h}|^2 \leq 4, i = 1, \dots, n+k\}. \end{aligned}$$

Specifically, suppose that there are two points that satisfy the constraint in (3.4). Then, there exist $\mathbf{h}_1 \in \mathbb{R}^{n+k}$ and $\mathbf{h}_2 \in \mathbb{R}^{n+k}$ such that $\mathbf{L}_1 \mathbf{h}_1 = \mathbf{L}_1 \mathbf{h}_2 = \mathbf{y}$, $|\mathbf{F}_i^H \mathbf{h}_1|^2 \leq 1, i = 1, \dots, n+k$, and $|\mathbf{F}_i^H \mathbf{h}_2|^2 \leq 1, i = 1, \dots, n+k$. Thus, we have $\mathbf{L}_1(\mathbf{h}_1 - \mathbf{h}_2) = \mathbf{0}$, and $|\mathbf{F}_i^H(\mathbf{h}_1 - \mathbf{h}_2)|^2 \leq 4, i = 1, \dots, n+k$. As a result, $\mathbf{C}_1 \cap \mathbf{C}_2 = \{\mathbf{0}\}$ is a sufficient condition to ensure the uniqueness of the solution.

In this paper, we prove that for sufficiently large k , and any $\mathbf{h} \in \mathbf{C}_2$, the following inequality holds with probability 1:

$$(3.5) \quad (c_1(n, k, \mathbf{x}) - \delta) \|\mathbf{h}\|_2^2 \leq \frac{1}{k} \|\mathbf{L}_1 \mathbf{h}\|_2^2 \leq (c_2(n, k, \mathbf{x}) + \delta) \|\mathbf{h}\|_2^2,$$

where $c_1(n, k, \mathbf{x}) > \delta$, $\delta \in (0, 1)$, $c_1(n, k, \mathbf{x})$ and $c_2(n, k, \mathbf{x})$ are two constants that depend on n, k and the ground truth \mathbf{x} . This implies that $\mathbf{C}_1 \cap \mathbf{C}_2 = \{\mathbf{0}\}$. As a result, we can conclude that the intersection of \mathbf{A} and \mathbf{B} contains only one point. This verifies that (3.1) and (3.4) have the same solution.

Remark 3.7. The formulation of (3.5) is similar to the Restricted Isometry Property (RIP) property [39], which is a standard analysis tool in Compressive Sensing (CS). However (3.4) is different. First, in CS, the signal of interest \mathbf{h} is usually assumed to be s -sparse, i.e., $\|\mathbf{h}\|_0 \leq s$, whereas in this paper, the Fourier spectrum of \mathbf{h} is not large than 1 at $\omega = \frac{2\pi l}{n+k}, l = 0, 1, \dots, n+k-1$. By Parseval's theorem, we can also find that $|\mathbf{F}_i^H \mathbf{h}|^2 \leq 4, i = 1, \dots, n+k$. Second, compared to the partial circulant Gaussian matrix analyzed in the RIP [40, 41, 42], some of the elements in \mathbf{L}_1 are not random, so the techniques used to prove the theorem will be different. In summary, we only need to prove the theory below.

THEOREM 3.8 (F-RIP). *For the phase retrieval with background information model, assume $\mathbf{x} \in \mathbb{R}^n$ is given, if $k > \max \left\{ \frac{n}{1-\delta}, \frac{8c\|\mathbf{x}\|_2}{\delta\sqrt{\eta}}, \frac{16c(\sqrt{\delta}+2)^2 \log(\frac{1}{\eta})}{\delta^2}, c(n, \delta) \right\}$, c is a constant and $c(n, \delta)$ is a constant depending on the n and δ , then with probability at least $1 - \eta$, the event that*

$$(3.6) \quad (c_1(n, k, \mathbf{x}) - \delta) \|\mathbf{h}\|_2^2 \leq \frac{1}{k} \|\mathbf{L}_1 \mathbf{h}\|_2^2 \leq (c_2(n, k, \mathbf{x}) + \delta) \|\mathbf{h}\|_2^2, \quad \forall \mathbf{h} \in \mathbf{C}_2$$

is held, where $\mathbf{C}_2 = \{\mathbf{h} \mid \|\mathbf{F}_i^H \mathbf{h}\|^2 \leq 4, i = 1, \dots, n+k\}$, $c_1(n, k, \mathbf{x}) > \delta$, $\delta \in (0, 1)$, $c_1(n, k, \mathbf{x})$ and $c_2(n, k, \mathbf{x})$ are two constants that depend on n, k and the ground truth \mathbf{x} .

To prove Theorem 3.8, we need to bound the spectral constant of \mathbf{L}_1 . Let $\mathbf{D} := \{\mathbf{h} \in \mathbb{R}^{n+k} : \|\mathbf{h}\|_2 \leq 1, \mathbf{h} \in \mathbf{C}_2\}$, we have

$$\begin{aligned} \delta_s &= \sup_{\mathbf{h} \in \mathbf{D}} \left| \langle (\mathbf{V}_z^H \mathbf{V}_z - c_1(n, k) \mathbf{I} - \Phi^H \Phi) \mathbf{h}, \mathbf{h} \rangle \right| = \sup_{\mathbf{h} \in \mathbf{D}} \left| \frac{1}{k} \|\mathbf{L}_1 \mathbf{h}\|_2^2 - c_1(n, k) \|\mathbf{h}\|_2^2 - \|\Phi \mathbf{h}\|_2^2 \right| \\ &= \sup_{\mathbf{h} \in \mathbf{D}} \left| \|\mathbf{V}_z \mathbf{h}\|_2^2 - c_1(n, k) \|\mathbf{h}\|_2^2 - \|\Phi \mathbf{h}\|_2^2 \right|, \end{aligned}$$

where $\mathbf{V}_z := \frac{1}{\sqrt{k}} \mathbf{P}_\Omega \mathbf{F}^{-1} \hat{\mathbf{Z}} \mathbf{F}$, and $\Phi := \frac{1}{\sqrt{k}} \mathbf{P}_\Omega \mathbf{F}^{-1} \hat{\mathbf{Z}}_1 \mathbf{F}$, where $\hat{\mathbf{Z}}_1$ is the Fourier transform of $\mathbf{z}_1 = [\mathbf{x}; \mathbf{0}] \in \mathbb{R}^{n+k}$. The second equality $\frac{1}{k} \|\mathbf{L}_1 \mathbf{h}\|_2^2$ is derived by

$$\begin{aligned} \frac{1}{k} \|\mathbf{L}_1 \mathbf{h}\|_2^2 &= \frac{1}{k} \langle \mathbf{L}_1^T \mathbf{L}_1 \mathbf{h}, \mathbf{h} \rangle = \frac{1}{k} \langle \mathbf{L}^T \mathbf{P}_\Omega^T \mathbf{P}_\Omega \mathbf{L} \mathbf{h}, \mathbf{h} \rangle \\ &= \frac{1}{k} \langle (\mathbf{F}^{-1} \hat{\mathbf{Z}} \mathbf{F})^T \mathbf{P}_\Omega^T \mathbf{P}_\Omega \mathbf{F}^{-1} \hat{\mathbf{Z}} \mathbf{F} \mathbf{h}, \mathbf{h} \rangle \\ &= \langle \mathbf{V}_z^H \mathbf{V}_z \mathbf{h}, \mathbf{h} \rangle. \end{aligned}$$

To perform analysis, $\mathbf{V}_z \mathbf{h}$ is divided into two parts: the first contains random elements \mathbf{y} , and the second contains non-random elements \mathbf{x} .

$$\begin{aligned} \mathbf{V}_z \mathbf{h} &= \frac{1}{\sqrt{k}} \mathbf{P}_\Omega \mathbf{F}^{-1} \hat{\mathbf{Z}} \mathbf{F} \mathbf{h} = \frac{1}{\sqrt{k}} \mathbf{P}_\Omega \mathbf{F}^{-1} \hat{\mathbf{H}} \mathbf{F} \mathbf{z} \\ &= \frac{1}{\sqrt{k}} \mathbf{P}_\Omega \mathbf{F}^{-1} \hat{\mathbf{H}} \mathbf{F}_1 \mathbf{x} + \frac{1}{\sqrt{k}} \mathbf{P}_\Omega \mathbf{F}^{-1} \hat{\mathbf{H}} \mathbf{F}_2 \mathbf{y}. \end{aligned}$$

Based on this, we have

$$\begin{aligned} \|\mathbf{V}_z \mathbf{h}\|_2^2 &= \left\| \frac{1}{\sqrt{k}} \mathbf{P}_\Omega \mathbf{F}^{-1} \hat{\mathbf{H}} \mathbf{F}_1 \mathbf{x} + \frac{1}{\sqrt{k}} \mathbf{P}_\Omega \mathbf{F}^{-1} \hat{\mathbf{H}} \mathbf{F}_2 \mathbf{y} \right\|_2^2 \\ &= \|\Phi \mathbf{h}\|_2^2 + \frac{1}{k} \|\mathbf{P}_\Omega \mathbf{F}^{-1} \hat{\mathbf{H}} \mathbf{F}_2 \mathbf{y}\|_2^2 + \frac{1}{k} \left(\left(\mathbf{P}_\Omega \mathbf{F}^{-1} \hat{\mathbf{H}} \mathbf{F}_1 \mathbf{x} \right)^H \mathbf{P}_\Omega \mathbf{F}^{-1} \hat{\mathbf{H}} \mathbf{F}_2 \mathbf{y} \right). \end{aligned}$$

Notice that

$$\begin{aligned} \frac{1}{k} \mathbb{E} \|\mathbf{P}_\Omega \mathbf{F}^{-1} \hat{\mathbf{H}} \mathbf{F}_2 \mathbf{y}\|_2^2 &= \frac{1}{k} \mathbb{E} \|\mathbf{P}_\Omega \mathbf{F}^{-1} \hat{\mathbf{H}} \mathbf{F} \tilde{\mathbf{y}}\|_2^2 \\ (3.7) \quad &= \frac{1}{k} \sum_{\ell=n+1}^{n+k} \sum_{i,j=1}^{n+k} \mathbb{E} \tilde{y}_j \tilde{y}_i h_{\ell-j} h_{\ell-i} = \frac{1}{k} \sum_{\ell=n+1}^{n+k} \sum_{i=n+1}^{n+k} |h_{\ell-i}|^2 = c_1(n, k) \|\mathbf{h}\|_2^2, \end{aligned}$$

where $\tilde{y}_i = 0, i = 1, 2, \dots, n$, $h_i = h_{n+k+i}, i = -n-k+1, -n-k, \dots, 0$ and $c_1(n, k)$ is a constant depending on the k and n . Specifically,

$$\begin{aligned} \frac{1}{k} \sum_{\ell=n+1}^{n+k} \sum_{i=n+1}^{n+k} |h_{\ell-i}|^2 &= \frac{1}{k} \sum_{\ell=n+1}^{n+k} \sum_{i=1}^{n+k} |h_{\ell-i}|^2 - \frac{1}{k} \sum_{\ell=n+1}^{n+k} \sum_{i=1}^n |h_{\ell-i}|^2 \\ &\geq \frac{1}{k} (k \|\mathbf{h}\|_2^2 - n \|\mathbf{h}\|_2^2). \end{aligned}$$

So $c_1(n, k) \geq \frac{k-n}{k}$.

As a result, δ_s can be bounded by the two terms as followings:

$$\begin{aligned} \delta_s &= \sup_{\mathbf{h} \in \mathbf{D}} \left| \frac{1}{k} \|\mathbf{P}_\Omega \mathbf{F}^{-1} \hat{\mathbf{H}} \mathbf{F}_2 \mathbf{y}\|_2^2 + \frac{1}{k} \left(\left(\mathbf{P}_\Omega \mathbf{F}^{-1} \hat{\mathbf{H}} \mathbf{F}_1 \mathbf{x} \right)^H \mathbf{P}_\Omega \mathbf{F}^{-1} \hat{\mathbf{H}} \mathbf{F}_2 \mathbf{y} \right) - c_1(n, k) \|\mathbf{h}\|_2^2 \right| \\ &\leq \underbrace{\sup_{\mathbf{h} \in \mathbf{D}} \left| \frac{1}{k} \|\mathbf{P}_\Omega \mathbf{F}^{-1} \hat{\mathbf{H}} \mathbf{F}_2 \mathbf{y}\|_2^2 - \frac{1}{k} \mathbb{E} \|\mathbf{P}_\Omega \mathbf{F}^{-1} \hat{\mathbf{H}} \mathbf{F}_2 \mathbf{y}\|_2^2 \right|}_{(1)} + \underbrace{\sup_{\mathbf{h} \in \mathbf{D}} \left| \frac{1}{k} \left(\mathbf{P}_\Omega \mathbf{F}^{-1} \hat{\mathbf{H}} \mathbf{F}_1 \mathbf{x} \right)^H \mathbf{P}_\Omega \mathbf{F}^{-1} \hat{\mathbf{H}} \mathbf{F}_2 \mathbf{y} \right|}_{(2)}. \end{aligned}$$

The first term (1) in the inequality above can be bounded by using the Chaos process techniques. Define $\mathbf{V}_\mathbf{h} := \frac{1}{\sqrt{k}} \mathbf{P}_\Omega \mathbf{F}^{-1} \hat{\mathbf{H}} \mathbf{F}_2$, and prove that

$$(3.8) \quad \sup_{\mathbf{h} \in \mathbf{D}} \left| \|\mathbf{V}_\mathbf{h} \mathbf{y}\|_2^2 - \mathbb{E} \|\mathbf{V}_\mathbf{h} \mathbf{y}\|_2^2 \right| := \delta_{s_1} \leq \frac{\delta}{2},$$

with probability at least $1 - \eta$, if $k > \max \left\{ \frac{16c(\sqrt{\delta}+2)^2 \log(\frac{1}{\eta})}{\delta^2}, c(n, \delta) \right\}$, where $\delta \in (0, 1)$, and c is a constant.

For the last term (2), by using the Chebyshev inequality, if $k \geq \frac{8c\|\mathbf{x}\|_2}{\delta\sqrt{\eta}}$,

$$(3.9) \quad \sup_{\mathbf{h} \in \mathbf{D}} \left| \frac{1}{k} \left(\mathbf{P}_\Omega \mathbf{F}^{-1} \hat{\mathbf{H}} \mathbf{F}_1 \mathbf{x} \right)^H \mathbf{P}_\Omega \mathbf{F}^{-1} \hat{\mathbf{H}} \mathbf{F}_2 \mathbf{y} \right| \leq \frac{\delta}{2},$$

with probability at least $1 - \eta$.

The proof of (3.8), (3.9) can be found in Appendix. Combing (3.8), (3.9), and the definition of δ_s , Theorem 3.9 can bound the norm of $\frac{1}{\sqrt{k}} \mathbf{L}_1 \mathbf{h}$.

THEOREM 3.9. *Let the background information $\mathbf{y} = \{y_1, y_2, \dots, y_n\}$ be a random vector with entries that satisfy the normal distribution. If, for any n , and $\eta, \delta \in (0, 1)$,*

$$k > \max \left\{ \frac{n}{1-\delta}, \frac{8c\|\mathbf{x}\|_2}{\delta\sqrt{\eta}}, \frac{16c(\sqrt{\delta}+2)^2 \log(\frac{1}{\eta})}{\delta^2}, c(n, \delta) \right\},$$

where c is a constant and $c(n, \delta)$ is a constant depending on the n and δ , then with probability at least $1 - \eta$,

$$(c_1(n, k) - \delta) \|\mathbf{h}\|_2^2 + \|\Phi \mathbf{h}\|_2^2 \leq \frac{1}{k} \|\mathbf{L}_1 \mathbf{h}\|_2^2 \leq (c_1(n, k) + \delta) \|\mathbf{h}\|_2^2 + \|\Phi \mathbf{h}\|_2^2, \mathbf{h} \in \mathbf{D},$$

where $c_1(n, k)$ is the constant in (3.7), and $c_1(n, k) > \delta$.

We can see that $\|\mathbf{L}_1 \mathbf{h}\|_2^2 = 0$ if and only if $\mathbf{h} = \mathbf{0}$. Under this condition, we can prove that $\mathbf{C}_1 \cap \mathbf{D} = \{\mathbf{0}\}$. For $\mathbf{h} \in \mathbf{C}_2 \setminus \mathbf{D}$, we have

$$\left| \mathbf{F}_i^H \left(\frac{\mathbf{h}}{\|\mathbf{h}\|_2} \right) \right|^2 \leq |\mathbf{F}_i^H \mathbf{h}|^2 \leq 4, \quad i = 1, \dots, n+k,$$

which implies that $\frac{\mathbf{h}}{\|\mathbf{h}\|_2} \in \mathbf{D}$. Thus, we can generalize Theorem 3.9 from \mathbf{D} to \mathbf{C}_2 , and Theorem 3.8 is proven.

Remark 3.10. To maintain that (3.1) and (3.4) have the same solution, more background information is usually required than to ensure the solution of (3.1) is uniquely defined. This can also be verified through numerical tests in subsection 4.1, as shown in Theorem 3.9.

Now that we have shown that the solution to (3.4) is equivalent to (3.1), we can use a series of convex methods to solve (3.4) and find the ground truth. For consistency, we propose a method called the Background Douglas-Rachford (CBDR) method. Similarly, we define

$$\mathbf{A} := \{\mathbf{z} \in \mathbb{R}^{n+k} : |\mathbf{F}^H \mathbf{z}| \leq \mathbf{b}^{\frac{1}{2}}\}$$

$$\mathbf{B} := \{\mathbf{z} \in \mathbb{R}^{n+k} : z_{n+i} = y_i, i = 1, \dots, k\}.$$

And the details of the CBDR are shown in Algorithm 3.2.

Algorithm 3.2 The Convex Background Douglas Rachford method

Input: $\{\mathbf{b}, \mathbf{y}, \varepsilon, T\}$

\mathbf{b} : the intensity only Fourier measurement.

\mathbf{y} : the background information.

ε : the allowed error bound.

T : the maximum allowed iteration.

Output:

$\bar{\mathbf{x}}$: an estimation of the real signal \mathbf{x} .

Initialization :

- 1: $\mathbf{z}^0 = \mathbb{P}_{\mathbf{B}}(\frac{1}{n+k} \mathbf{F} \cdot \mathbf{b}^{\frac{1}{2}})$, $\mathbf{B} = \{\mathbf{z} : z_{n+i} = y_i, i = 1, \dots, k\}$.
- 2: $p = 1$.

General step

- 1: $\tilde{\mathbf{z}}^{p-1} = \mathbb{P}_{\mathbf{A}}(\mathbf{z}^{p-1})$, where $\mathbf{A} = \{\mathbf{z} : |\mathbf{F}^H \mathbf{z}| \leq \mathbf{b}^{\frac{1}{2}}\}$
 - 2: $z_t^p = \tilde{z}_t^{p-1}, t = 1, \dots, n$,
 - $z_{n+t}^p = \tilde{z}_{n+t}^{p-1} - \tilde{z}_{n+t}^{p-1} + y_t, t = 1, \dots, k$.
 - 3: **if** $\|\mathbf{z}^p - \mathbf{z}^{p-1}\|_2 \leq \varepsilon$ **or** $p = T + 1$ **then**
 - 4: $\bar{\mathbf{z}} = \mathbf{z}^p$.
 - 5: $\bar{\mathbf{x}} = [\bar{z}_1, \bar{z}_2, \dots, \bar{z}_n]^T$
 - 6: Break.
 - 7: **end if**
 - 8: $p = p + 1$
-

Compared to Algorithm 3.1, the main difference in Algorithm 3.2 is the operator $\mathbb{P}_{\mathbf{A}}(\cdot)$. In Algorithm 3.2, $\tilde{\mathbf{z}}^{p-1}$ is the projection of \mathbf{z}^{p-1} onto \mathbf{A} . We define $\hat{\mathbf{z}}^{p-1}$ and $\hat{\mathbf{z}}^{p-1}$ as the Fourier transforms of $\tilde{\mathbf{z}}^{p-1}$ and \mathbf{z}^{p-1} , respectively, which have the following property:

$$(3.10) \quad \hat{z}_i^{p-1} = \begin{cases} b_i^{\frac{1}{2}} \frac{\hat{z}_i^{p-1}}{|\hat{z}_i^{p-1}|}, & \text{if } |\hat{z}_i^{p-1}| \geq b_i^{\frac{1}{2}} \\ |\hat{z}_i^{p-1}| \frac{\hat{z}_i^{p-1}}{|\hat{z}_i^{p-1}|}, & \text{if } |\hat{z}_i^{p-1}| < b_i^{\frac{1}{2}} \end{cases}.$$

Then, the convergence of the CBDR method can be proved by the Theorem by using the theoretical results in [43].

THEOREM 3.11. *Suppose that $\mathbf{A} \cap \mathbf{B} \neq \emptyset$. Then the sequence $\{\mathbf{z}^p\}$ generated by the Algorithm 3.2 has the property that $\|\mathbf{z}^p - \bar{\mathbf{z}}\|_2 \rightarrow 0$ as p increases and $\mathbb{P}_{\mathbf{B}}(\{\mathbf{z}^p\}) \rightarrow \mathbb{P}_{\mathbf{B}}(\bar{\mathbf{z}}) \in \mathbf{A} \cap \mathbf{B}$, where $\bar{\mathbf{z}}$ is one of the fixed points of the CBDR method.*

When $\mathbf{z} \in \mathbb{R}^n$, we can further restrict the feasible set \mathbf{A} and search for signals of interest by performing two parallel tasks. Specifically, we apply CBDR method on $\{\mathbf{A}_1, \mathbf{B}\}$, and $\{\mathbf{A}_2, \mathbf{B}\}$ simultaneously, where

$$\mathbf{A}_1 := \{\mathbf{z} \in \mathbb{R}^{n+k} : |\mathbf{F}_i^H \mathbf{z}| \leq b_i^{\frac{1}{2}}, i = 2, 3, \dots, n+k, \sum_{i=1}^{n+k} z_i = \sqrt{b_1}\},$$

and

$$\mathbf{A}_2 := \{\mathbf{z} \in \mathbb{R}^{n+k} : |\mathbf{F}_i^H \mathbf{z}| \leq b_i^{\frac{1}{2}}, i = 2, 3, \dots, n+k, \sum_{i=1}^{n+k} z_i = -\sqrt{b_1}\}.$$

The final estimation is the one with the least measurement error.

4. Numerical test. In this section, we will compare the BDR method with the PGD method. In all tests, the background information is generated using the Gaussian distribution. The tests were conducted on a Dell desktop with a 2.70 GHz Intel Core i7 processor and 32GB DDR3 memory.

The relative error is defined as

$$(4.1) \quad e = \frac{\|\bar{\mathbf{x}} - \mathbf{x}\|_2}{\|\mathbf{x}\|_2},$$

where $\bar{\mathbf{x}}$ is the estimation for the ground truth \mathbf{x} .

The measurement error is defined as

$$me = \frac{\| |\mathbf{F}^H \bar{\mathbf{z}}|^2 - \mathbf{b} \|_2}{\|\mathbf{b}\|_2},$$

where $\bar{\mathbf{z}} = [\bar{\mathbf{x}}; \mathbf{y}]$. The length of the 1-D signals used in this test is 100. The size of the 2-D images is 256×256 . In all numerical tests, the Fourier measurements have no oversampling, namely $m_i = n_i + k_i, i = 1, 2$.

4.1. Phase transition of different methods. First, we analyze the phase transition where the recovery rate is above 90% for the PGD, CBDR and BDR methods. The signal of interest is $\mathbf{x} \stackrel{\text{i.i.d}}{\sim} \mathcal{N}(\mathbf{0}, \mathbf{I})$. The length of the signal ranges from 100 to 1000 with an interval of 5. For each signal, measurements \mathbf{b} are generated by (3.1) with k/n ranging from 1 to 7 with an interval of 0.1. Then, we apply the PGD, CBDR and BDR methods to recover the signal. A relative error below 10^{-5} is considered a successful recovery. The test are repeated 100 times for each n and k/n . The results are shown in Fig 4.

In Fig 4, the figures from left to right represent the results calculated by the PGD, CBDR and BDR methods. The corresponding red line is the phase transition where the recovery rate is above 90%. We observe that the BDR method requires the least background information to achieve the highest recovery rate, followed by the CBDR method. This demonstrates that the DR method is more likely to find the ground truth when the background information is sufficient. Additionally, we depict the phase transition of the BDR method where the recovery rate is above 99% with a dashed red line. The mean of the dashed red line is 2.76. These results reflect the superiority of BDR method which can recover the signal of interest when k/n is approximately equal to the theoretical bound of 3.

Although CBDR method is complete in theory, it still requires $k/n \approx 5.5$ for a higher recovery rate in practice. This is because convexity may introduce some

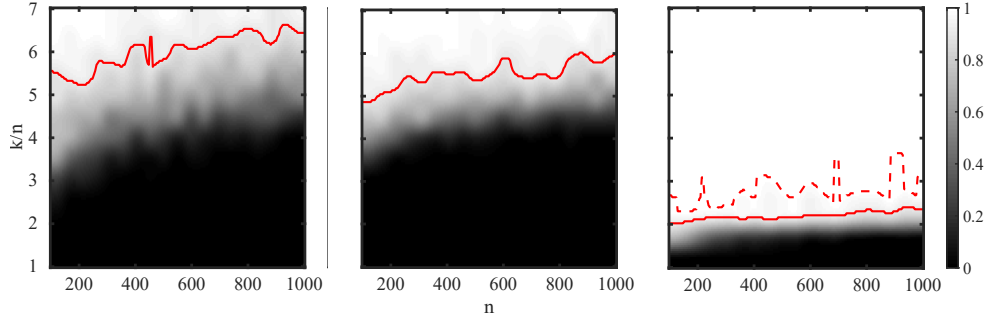


Fig. 4: The phase transition of the PGD, CBDR and BDR methods. The figures from left to right represent the results calculated by the PGD, CBDR and BDR methods. The corresponding red line is the phase transition where the recovery rate is above 90%. The dashed red line depicts the phase transition where the recovery rate is above 99% for the BDR method.

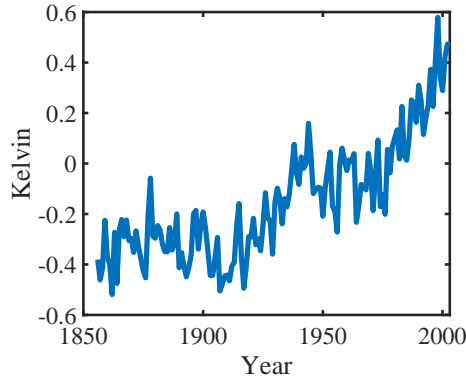


Fig. 5: The annual mean global surface temperature anomaly.

spurious points into the feasible solutions, and more background information is necessary to mitigate this issue. However, CBDR’s performance is still better than that of the PGD method. The BDR and CBDR methods both use the Douglas-Rachford method as their backbone. Therefore, in the remaining sections, we will focus only on the BDR method, which can achieve better performance.

4.2. The effect of the length of signal. First, we consider 1-D signals of three different types in the test.

- Type 1: $\mathbf{x} \stackrel{\text{i.i.d}}{\sim} \mathcal{N}(\mathbf{0}, \mathbf{I})$
- Type 2: $f(t) = \cos(39.2\pi t - 12\sin 2\pi t) + \cos(85.4\pi t + 12\sin 2\pi t)$, $t \in (0, 1)$
- Type 3: the annual mean global surface temperature anomaly which can be seen in Fig.5

Background information is generated for each signal, and its corresponding Fourier amplitude only spectrum is measured. k/n ranges from 1 to 7 with an interval of 0.1. At each k/n , the PR test is applied 100 times with different \mathbf{y} . The maximum

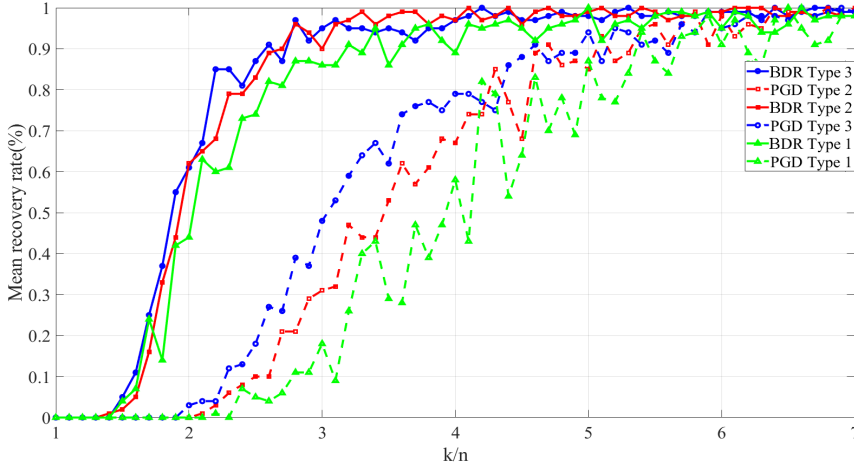


Fig. 6: The mean recovery rate of BDR and PGD method. The signal has 3 different types. Type 1 is the random signal, type 2 is the harmonic signal, type 3 is the structure signal.

iteration of both the BDR and PGD methods is 300. Success is judged if the relative error e is below 10^{-5} . The empirical recovery rate at each k is calculated as the total successful recovery times divided by 100. Figure 6 shows the results of the test.

According to Figure 6, the BDR method has a higher recovery rate than PGD. Specifically, when $k/n = 3$, the BDR method achieves a recovery rate larger than 85%, which is close to the theoretical bound of $3n - 1$, while the recovery rate of PGD remains below 40%.

In Figure 7, we observe that the signal recovered by the BDR method fits the ground truth well, while the PGD method fails to recover the outline of the signal. Moreover, the relative error and measurement error of the BDR method decrease rapidly, while the PGD method stagnates at a local minimum. Even when $k/n = 2$, the BDR method still achieves a recovery rate of approximately 60%, while the PGD method fails to recover any type of signal.

These results fully demonstrate the ability of BDR to alleviate the effect of the stagnation point. It is worth noting that type 1 signals (random signals) are harder to recover than type 2 (determined signals) and type 3 signals (signals with structure). However, in real-life applications, the signal of interest is usually not completely random, which suggests that the BDR method may perform well in practice.

Next, we will test the ability of the BDR method to deal with the 2-D images. The index of peak signal to noise ratio (PSNR) and the structure similarity index (SSIM) are chosen as the criterion to judge the performance of recovery. The time cost by each methods is also recorded. The test pictures are shown in Figure 8. In each dimension, background information is k/n folds of the object. At each k/n ratio, we record the recovered images' PSNR, SSIM and time under 100 different background information. Each test is applied with 300 iterations. If the relative error is below 10^{-5} , we stop the iterate in advance. All the images are in the center of the background information. The results are shown in Figure 9.

From Figure 9, we can find that the medium of the PSNR and SSIM of the BDR method is higher than the PGD method. Especially when $k/n = 0.6$, which is

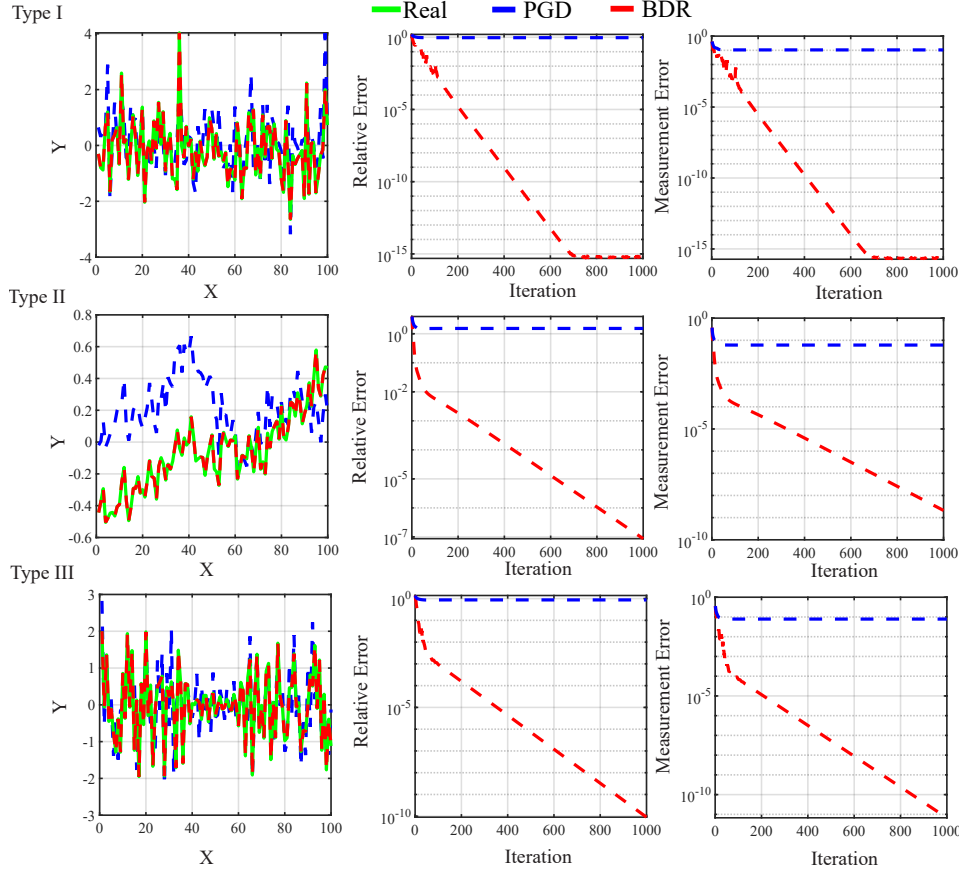


Fig. 7: Comparisons of BDR and PGD method when $k/n = 3$. The first column displays the comparison between the signals recovered by the PGD method and the BDR method. The second column and last column shows the relative error and measurement error of the results in the first column respectively.

mostly smaller than the uniqueness bound required in Theorem 2.1, the medium of the PSNR for the BDR method is above 60dB, but the medium of PSNR for PGD is below 30dB. Figure 9 indicates that the BDR method can have a good performance when less background information is available. At the same time, we can also find that the variance of the PSNR and SSIM for the BDR method is smaller than PGD method. This also shows that the BDR method can be more numerical stable. With k/n increasing, the time demanded by BDR method is more than PGD method. But when $k/n \leq 1$, the time cost by both methods is nearly the same, but BDR method can perform better judging from the PSNR and SSIM.

4.3. The robustness test. This subsection describes experiments to test the robustness of the BDR algorithm to the locations of the background information and the measurement noise.

Firstly, the influence of the locations of the background information is tested. The sample 'Baboon' is to be recovered with $k/n = 2$. Seventeen different positions

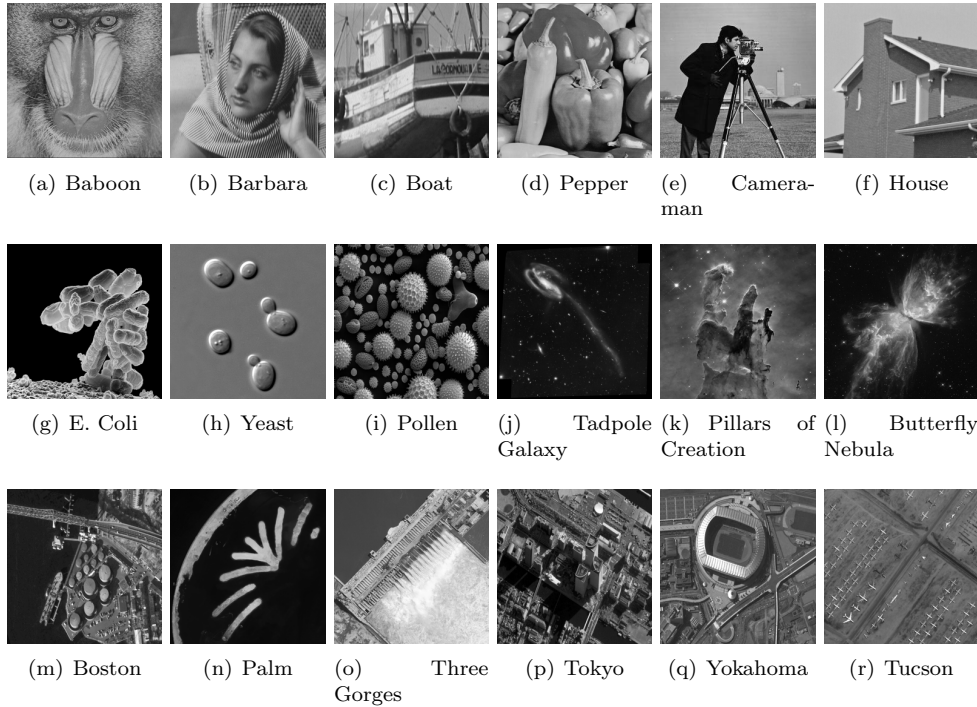


Fig. 8: We attempt to reconstruct 16 test images, including (a-f) natural images, (g-l) astronomy and microbe pictures from Wikipedia under public domain licenses, and (m-r) remote sensing pictures.

of Baboon are selected, from the left corner to the center in Figure 10(a). At each position, tests are replicated by BDR 10 times. The mean PSNR, mean SSIM, and the mean relative error at each position are recorded (see Figure 10(b), 10(c), and 10(d)). In Figure 10(b), 10(c), and 10(d), the coordinate of each pixel indicates the location of the left-top of the Baboon in the combined picture. Due to the symmetry of positions, only four-ninths parts are considered in Figure 10(a).

As seen from Figure 10(a), similar to the PGD method in [1], the locations of the background information also affect the performance of the BDR method. Specifically, from the left corner to the center, SSIM and PSNR of the recovered image gradually increase. However, compared to PGD in [1], the BDR method is less sensitive to the locations of the background information.

Next, experiments are applied to test the robustness of the algorithm to the measurement noise for 2-D pictures. The noise model is given by:

$$\sqrt{b_i} = |\mathbf{F}_i^H \mathbf{z}| + \varepsilon_i, i = 1, \dots, m,$$

where ε_i is the Gaussian noise.

Five different single-channel pictures were selected as objects, and the BDR and PGD methods were used to recover these images from their noisy measurements. Table 2 shows the PSNR and SSIM of the recovered images. The results in Table 2 demonstrate that the BDR method is less robust to measurement noise than the

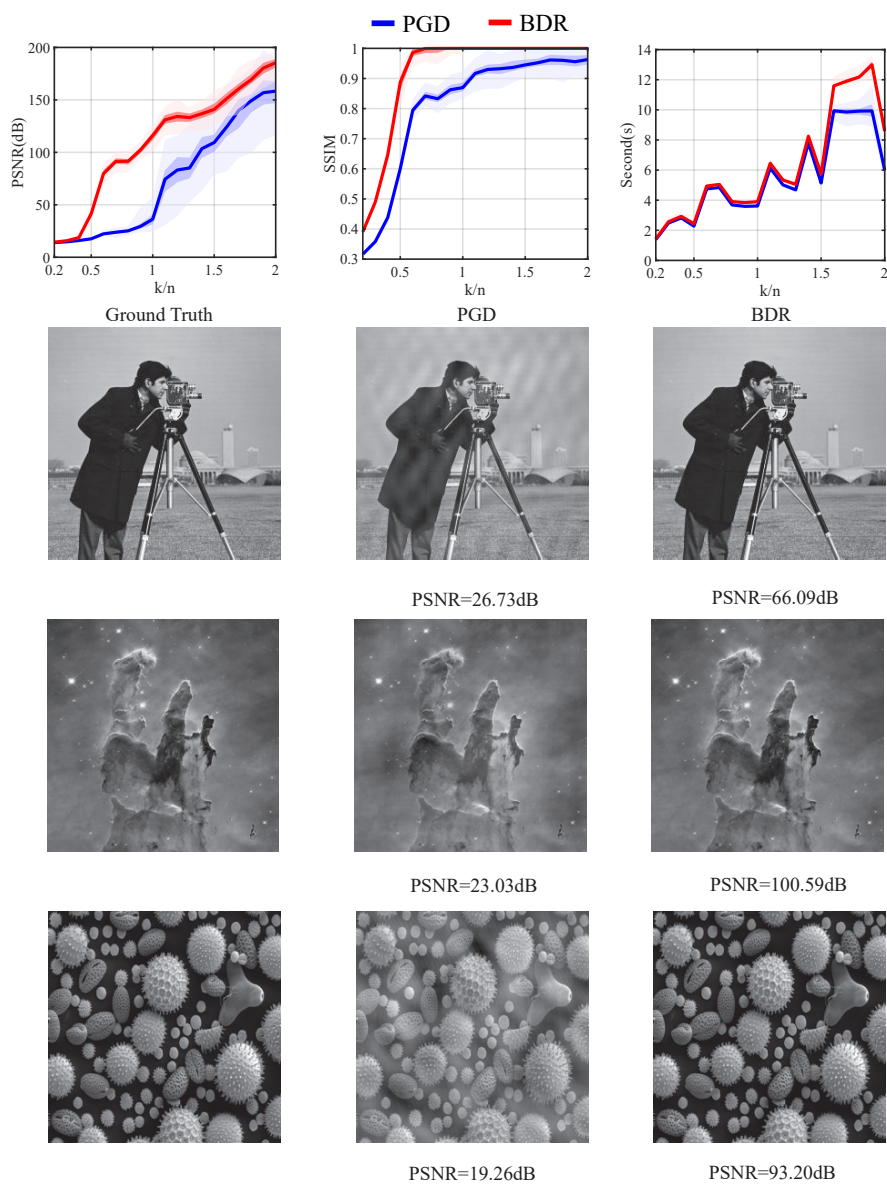


Fig. 9: The comparison between PGD and BDR methods for recovering 2D images is presented. In the first row, we compare PSNR, BDR, and time for PGD and BDR. The thick line represents the median over 100 trials, the light area represents the minimum and maximum values, and the darker area indicates the 25th and 75th quantiles. In rows 2-4, we show the results recovered by PGD and BDR when $n/k = 0.6$.

PGD method, but it requires less background information. To improve its ability to

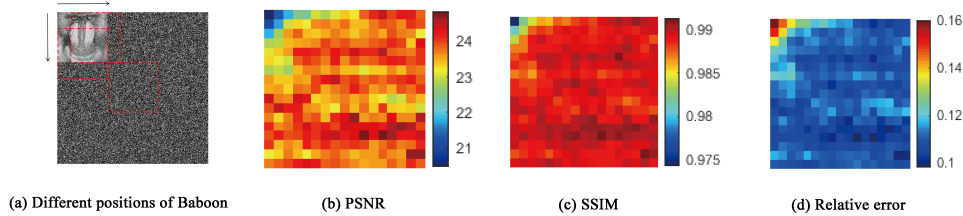


Fig. 10: Pictures recovered under different locations of the background information.

Table 2: Results for the robustness test of 2-D Fourier PR with background information, recovering noisy measurements.

		PSNR		SSIM		Relative error	
		$\sigma = 0.001$	$\sigma = 0.003$	$\sigma = 0.001$	$\sigma = 0.003$	$\sigma = 0.001$	$\sigma = 0.003$
Baboon	PGD	21.87	11.33	0.75	0.32	0.13	0.37
	BDR	19.78	10.45	0.66	0.25	0.17	0.38
	BDR1	22.23	12.28	0.76	0.33	0.12	0.37
Barba	PGD	17.91	14.03	0.64	0.34	0.20	0.38
	BDR	21.35	12.89	0.56	0.30	0.17	0.45
	BDR1	23.61	14.48	0.68	0.34	0.14	0.37
Lena	PGD	23.40	13.72	0.56	0.19	0.14	0.40
	BDR	21.12	12.58	0.44	0.14	0.18	0.46
	BDR1	23.60	14.35	0.58	0.20	0.13	0.38
Harbour	PGD	22.45	12.56	0.62	0.26	0.14	0.40
	BDR	20.31	11.61	0.52	0.20	0.18	0.41
	BDR1	22.25	12.45	0.63	0.26	0.13	0.39
Golden Hill	PGD	23.83	12.56	0.67	0.24	0.13	0.41
	BDR	21.50	11.61	0.54	0.18	0.17	0.46
	BDR1	23.85	11.45	0.68	0.25	0.12	0.37

resist noise, we adapted the third step of Algorithm 3.1 as follows:

$$\begin{aligned}
 z_t^p &= \tilde{z}_t^{p-1}, t = 1, \dots, n, \\
 z_{n+t}^p &= z_{n+t}^{p-1} - \beta \tilde{z}_{n+t}^{p-1} + y_t, t = 1, \dots, k,
 \end{aligned}$$

Here, β is a parameter that controls the projection. This modified algorithm is named BDR1. In the numerical test, we set $\beta = 0.9$. Table 2 shows that this adaptation can improve the robustness of the BDR algorithm and achieve better performance than the PGD method.

4.4. Empirical test of the background information model. Finally, a physical setup is built to demonstrate the capacity of the background information model for the PR problem.

As shown in Figure 11(b), a collimated and expanded laser beam with a wavelength of $\lambda = 632.8nm$ illuminates an object that is the symbol '5' from group 1 of the negative USAF 1951 target. The size of the object is 1.2 mm^4 . The object is manufactured by Edmund Optics. More details about the resolution targets can be found at

⁴We use the character '5', which is more complex than the vertical and horizontal 3 bars in the

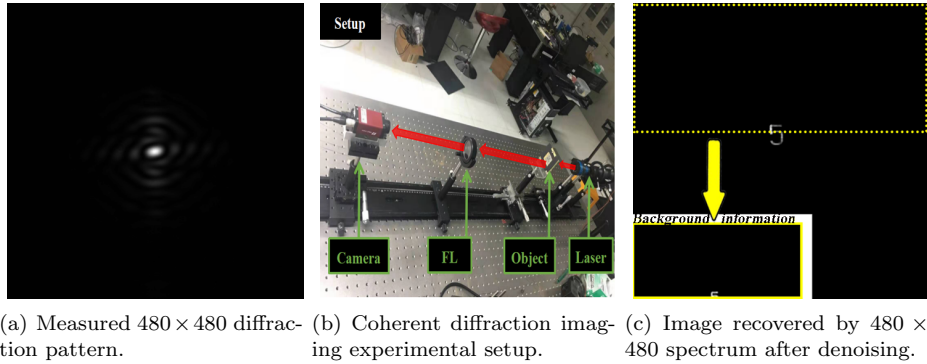


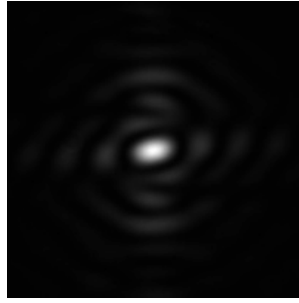
Fig. 11: Experiment setup: (a) shows the diffraction pattern measured by the CCD. (b) depicts the CDI setup. (c) displays the denoised image recovered by HIO. The yellow rectangle indicates the background information.

<https://www.edmundoptics.cn/p/2-x-2-negative-1951-usaf-hi-resolution-target/12479/#>. The laser beam is focused by an FT lens (with a focal length of $L = 300\text{mm}$ and diameter of $D = 30\text{mm}$). The diffraction pattern is captured by a CCD sensor (Point Grey Grasshopper2, with a pixel size of $6.45\mu\text{m}$ and 2048×2048 pixels) using a microscope objective (Newport, $\times 10$, $\text{NA}=0.25$). The microscope objective is placed at the rear focal plane of the FT lens. The exposure time is $5000\mu\text{s}$.

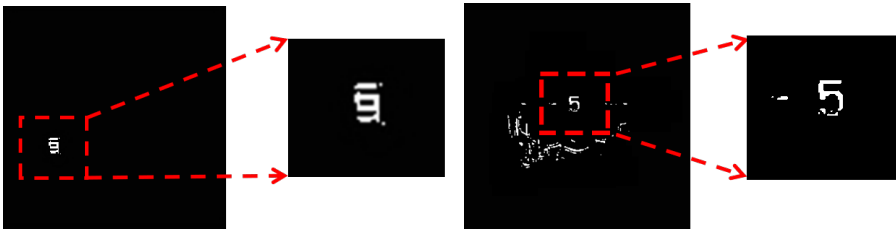
The captured diffraction pattern has a size of 480×480 , as shown in Figure 11(a). Using these raw data, we have reconstructed a clear image with the HIO algorithm, as shown in Figure 11(c). However, this reconstruction was based on a large bandwidth of the spectrum. It is crucial to devise a method to recover images with less frequency information. For the remaining tests, we assume that the obtained region of the spectrum is 200×200 , which can be seen in Figure 12(a). As shown in Figure 12(b), using the HIO algorithm on the 200×200 spectrum cannot reconstruct an identifiable object image due to the loss of high-frequency information. Using the same spectrum shown in Figure 12(a), we apply the background information model to recover the image. The background information, which is the part of the 200×200 image visible in Figure 11(c), has a length almost equal to $0.5n$. The BDR method is then applied to recover the image, and the results are displayed in Figure 12(c). We observe that the outline of the number '5' can be reconstructed from the 200×200 spectrum with the help of the background information. Although the quality of the image recovered by the BDR algorithm is not very high, this may be attributed to insufficient background information. Nonetheless, it effectively demonstrates the advantage of the background information model.

5. Conclusion. This paper focuses on studying the phase retrieval with background information model. Theoretical results demonstrate that the solution's uniqueness can be guaranteed with less background information for 2-D images as compared to previous works. Additionally, the uniqueness result for the general signal is also derived, and a bound between the estimation and the ground truth is established when

USAF 1951, because the purpose of this experiment is to test the BDR method's ability to recover the object from its diffraction pattern, not to test the resolution of the recovered object.



(a) 200×200 diffraction pattern which is cropped from Figure 11(a)



(b) The result of HIO from 200×200 spectrum after denoising.

(c) The result of BDR from 200×200 spectrum after denoising.

Fig. 12: Experiment results: (a) shows the diffraction pattern used to recover the image. (b) shows the result recovered via HIO. (c) shows the result recovered by the BDR method with the aid of the background information in Figure 11(c).

the measurement is corrupted by noise and suffers from the background information bias.

Two methods, BDR and CBDR, are proposed to find the ground truth. Theoretical results show that the BDR method can achieve an R-linear convergence rate if the initialization is close to the ground truth. Meanwhile, CBDR method can guarantee global convergence based on the satisfaction of the F-RIP property. Numerical simulations demonstrate the high efficiency of the BDR method, which requires less background information but offers better performance. Although the CBDR method have a better convergence guarantee, it requires more background information to avoid introducing extra solutions. The advantages of the background information model are further illustrated through the application of coherent diffraction imaging.

Acknowledgment. This work was supported by the National Natural Science Foundation of China (61977065), National Key Research and Development Program (2020YFA0713504). The authors would like to thank Prof. Xiujian Li and Dr. Wusheng Tang for assisting in the optical tests.

REFERENCES

- [1] Ziyang Yuan and Hongxia Wang. Phase retrieval with background information. *Inverse Problems*, 35(5):054003, 2019.
- [2] Jianwei Miao, Pambos Charalambous, Janos Kirz, and David Sayre. Extending the method-

- ology of x-ray crystallography to allow imaging of micrometre-sized non-crystalline specimens. *Nature*, 400(6742):342–344, 1999.
- [3] C Fienup and J Dainty. Phase retrieval and image reconstruction for astronomy. *Image Recovery: Theory and Application*, pages 231–275, 1987.
 - [4] Guoan Zheng, Roarke Horstmeyer, and Changhui Yang. Wide-field, high-resolution fourier ptychographic microscopy. *Nature photonics*, 7(9):739, 2013.
 - [5] Robert Beinert and Gerlind Plonka. Enforcing uniqueness in one-dimensional phase retrieval by additional signal information in time domain. *Applied and Computational Harmonic Analysis*, 2016.
 - [6] Philipp Grohs, Sarah Koppensteiner, and Martin Rathmair. Phase retrieval: Uniqueness and stability. *SIAM Review*, 62(2):301–350, 2020.
 - [7] Tamir Bendory, Robert Beinert, and Yonina C Eldar. Fourier phase retrieval: Uniqueness and algorithms. In *Compressed Sensing and its Applications*, pages 55–91. Springer, 2017.
 - [8] Robert Beinert and Gerlind Plonka. Ambiguities in one-dimensional discrete phase retrieval from fourier magnitudes. *Journal of Fourier Analysis and Applications*, 21(6):1169–1198, 2015.
 - [9] E. M. Hofstetter. Construction of time-limited functions with specified autocorrelation functions. *IEEE Transactions on Information Theory*, 10(2):119–126, 1964.
 - [10] M.H. Hayes. The reconstruction of a multidimensional sequence from the phase or magnitude of its fourier transform. *Acoustics Speech and Signal Processing IEEE Transactions on*, 30(2):140–154, 1982.
 - [11] J R Fienup. Phase retrieval algorithms: a comparison. *Applied Optics*, 21(15):2758–2769, 1982.
 - [12] R. W. Gerchberg. A practical algorithm for the determination of phase from image and diffraction plane pictures. *Optik*, 35:237–250, 1971.
 - [13] Zaiwen Wen, Chao Yang, Xin Liu, and Stefano Marchesini. Alternating direction methods for classical and ptychographic phase retrieval. *Inverse Problems*, 28(11):115010, 2012.
 - [14] D Russell Luke. Relaxed averaged alternating reflections for diffraction imaging. *Inverse problems*, 21(1):37–50, 2004.
 - [15] Heinz H Bauschke, Patrick L Combettes, and D Russell Luke. Hybrid projection–reflection method for phase retrieval. *JOSA A*, 20(6):1025–1034, 2003.
 - [16] Radu Balan, Pete Casazza, and Edidin Dan. On signal reconstruction without phase. *Applied and Computational Harmonic Analysis*, 20(3):345–356, 2006.
 - [17] E. J. Candes, Xiaodong Li, and M. Soltanolkotabi. Phase retrieval via wirtinger flow: Theory and algorithms. *IEEE Transactions on Information Theory*, 61(4):1985–2007, 2014.
 - [18] Philipp Grohs and Martin Rathmair. Stable gabor phase retrieval and spectral clustering. *Communications on Pure and Applied Mathematics*, 72(5):981–1043, 2019.
 - [19] Wooshik Kim and Monson H Hayes. Phase retrieval using two fourier-transform intensities. *JOSA A*, 7(3):441–449, 1990.
 - [20] Dirk Langemann and Manfred Tasche. Phase reconstruction by a multilevel iteratively regularized gauss–newton method. *Inverse problems*, 24(3):035006, 2008.
 - [21] Birger Seifert, Heinrich Stolz, Marco Donatelli, Dirk Langemann, and Manfred Tasche. Multilevel gauss–newton methods for phase retrieval problems. *Journal of Physics A: Mathematical and General*, 39(16):4191, 2006.
 - [22] Juri Ranieri, Amina Chebira, Yue M. Lu, and Martin Vetterli. Phase retrieval for sparse signals: Uniqueness conditions. *IEEE Transactions on Information Theory*, 2013.
 - [23] H. Ohlsson and Y. C. Eldar. On conditions for uniqueness in sparse phase retrieval. In *Acoustics, Speech and Signal Processing (ICASSP), 2014 IEEE International Conference on*, pages 1841 – 1845, 2013.
 - [24] Alexei Novikov and Stephen White. Support recovery for sparse multidimensional phase retrieval. *IEEE Transactions on Signal Processing*, 69:4403–4415, 2021.
 - [25] A Szameit, Y Shechtman, E Osherovich, E Bullkich, P Sidorenko, H Dana, S Steiner, E. B. Kley, S Gazit, and T Cohen-Hyams. Sparsity-based single-shot subwavelength coherent diffractive imaging. *Nature Materials*, 11(5):1 – 4, 2012.
 - [26] K. Jaganathan, S. Oymak, and B. Hassibi. Recovery of sparse 1-d signals from the magnitudes of their fourier transform. In *IEEE International Symposium on Information Theory*, pages 1473–1477, 2012.
 - [27] Yoav Shechtman, Andre Beck, and Yonina C. Eldar. Gespar: Efficient phase retrieval of sparse signals. *IEEE Transactions on Signal Processing*, 62(4):928–938, 2013.
 - [28] O Raz, N Dudovich, and B Nadler. Vectorial phase retrieval of 1-d signals. *IEEE Transactions on Signal Processing*, 61(7):1632–1643, 2013.
 - [29] David A Barmherzig, J. Sun, Emmanuel J Candes, T. J Lane, and P. N. Li. Holographic phase retrieval and optimal reference design. *Inverse Problems*, 35(9):094001, 2019.

- [30] Rakib Hyder, Zikui Cai, and M. Salman Asif. Solving phase retrieval with a learned reference. In Andrea Vedaldi, Horst Bischof, Thomas Brox, and Jan-Michael Frahm, editors, *Computer Vision – ECCV 2020*, pages 425–441, Cham, 2020. Springer International Publishing.
- [31] Jianwei Miao, David Sayre, and HN Chapman. Phase retrieval from the magnitude of the fourier transforms of nonperiodic objects. *JOSA A*, 15(6):1662–1669, 1998.
- [32] Bing Gao, Qiyu Sun, Yang Wang, and Zhiqiang Xu. Phase retrieval from the magnitudes of affine linear measurements. *Advances in Applied Mathematics*, 93:121–141, 2018.
- [33] Afonso S. Bandeira, Jameson Cahill, Dustin G. Mixon, and Aaron A. Nelson. Saving phase: Injectivity and stability for phase retrieval. *Applied and Computational Harmonic Analysis*, 37(1):106–125, 2013.
- [34] Aldo Conca, Dan Edidin, Milena Hering, and Cynthia Vinzant. An algebraic characterization of injectivity in phase retrieval. *Applied and Computational Harmonic Analysis*, 38(2):346–356, 2015.
- [35] X. Li and V. Voroninski. Sparse signal recovery from quadratic measurements via convex programming. *Siam Journal on Mathematical Analysis*, 45(5):3019–3033, 2012.
- [36] Victor Y. Pan and Guoliang Qian. Tr-2012013: Condition numbers of random toeplitz and circulant matrices. Technical report, CUNY Academic Works, 2012.
- [37] Hung M Phan. Linear convergence of the douglas–rachford method for two closed sets. *Optimization*, 65(2):369–385, 2016.
- [38] Meng Huang and Zhiqiang Xu. Strong convexity of affine phase retrieval. *arXiv preprint arXiv:2204.09412*, 2022.
- [39] Emmanuel J Candes and Terence Tao. Decoding by linear programming. *IEEE transactions on information theory*, 51(12):4203–4215, 2005.
- [40] Felix Krahmer, Shahar Mendelson, and Holger Rauhut. Suprema of chaos processes and the restricted isometry property. *Communications on Pure and Applied Mathematics*, 67(11):1877–1904, 2014.
- [41] Jarvis Haupt, Waheed U Bajwa, Gil Raz, and Robert Nowak. Toeplitz compressed sensing matrices with applications to sparse channel estimation. *IEEE transactions on information theory*, 56(11):5862–5875, 2010.
- [42] Holger Rauhut, Justin Romberg, and Joel A Tropp. Restricted isometries for partial random circulant matrices. *Applied and Computational Harmonic Analysis*, 32(2):242–254, 2012.
- [43] Heinz H Bauschke, Patrick L Combettes, and Luke D Russell. Phase retrieval, error reduction algorithm, and fienu variants: a view from convex optimization. *Journal of the Optical Society of America A Optics Image Science and Vision*, 19(7):1334–45, 2002.
- [44] Hayes M and Oppenheim A Lim J. Signal reconstruction from phase or magnitude. *IEEE Transactions on Acoustics, Speech, and Signal Processing*, 28(6):672–680, 2003.

Appendix A. The proof of Theorem 3.3. To prove the theoretical results, we introduce lemmas related to the set regularity.

DEFINITION A.1. *The proximal normal cone $N_{\Omega}^{\text{prox}}(\mathbf{z})$ to a set Ω at a point $\mathbf{z} \in \Omega$ is defined by*

$$N_{\Omega}^{\text{prox}}(\mathbf{z}) := \text{cone}(\mathbb{P}_{\Omega}^{-1}(\mathbf{z}) - \mathbf{z}),$$

where $\mathbb{P}_{\Omega}^{-1}(\mathbf{z})$ is the preimage set of $\mathbb{P}_{\Omega}(\cdot)$ under \mathbf{z} . Then the limiting normal cone or the Mordukhovich normal cone $N_{\Omega}(\mathbf{z})$ is defined as any vector that can be the limit of the proximal normal, namely

$$N_{\Omega}(\mathbf{z}) := \{\mathbf{u} \in \mathbb{R}^{n+k} \mid \exists \{\mathbf{z}^p\} \subset \Omega, \mathbf{u}^p \in N_{\Omega}^{\text{prox}}(\mathbf{z}^p) \text{ so that } \mathbf{z}^p \rightarrow \mathbf{z}, \mathbf{u}^p \rightarrow \mathbf{u}, \text{ as } p \rightarrow \infty\}.$$

Figure 13 provides a graphical illustration of the Mordukhovich normal cone. From its definition, we know that the limiting normal cone is the smallest cone that satisfies the following two properties:

- i. $\mathbb{P}_{\Omega}^{-1}(\mathbf{z}) \subseteq (\mathbb{I} + N_{\Omega})(\mathbf{z})$.
- ii. For any sequence $\mathbf{z}^p \rightarrow \mathbf{z}$, where $\{\mathbf{z}^p\} \in \Omega$, if $\mathbf{u}^p \in N_{\Omega}(\mathbf{z}^p)$ converges to \mathbf{u} as $p \rightarrow \infty$, then \mathbf{u} must lie in $N_{\Omega}(\mathbf{z})$.

Next, we will introduce some definitions about the regularity of a set. These definitions can help us analyze the convergence rate.

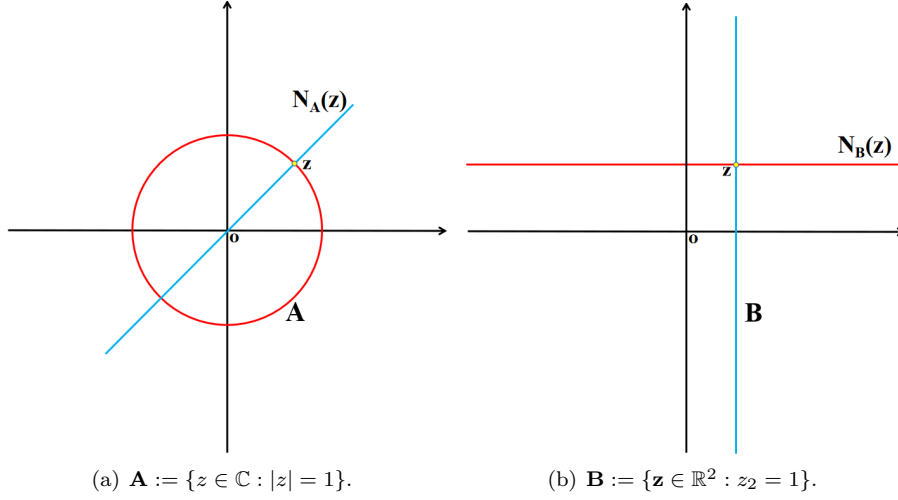


Fig. 13: The graphical illustration of the Mordukhovich normal cone.

DEFINITION A.2 (Regularity of set systems). *Let \mathbf{A} and \mathbf{B} be two subsets of \mathbb{R}^{n+k} and let $\mathbf{z} \in \mathbf{A} \cap \mathbf{B}$. We say that the system $\{\mathbf{A}, \mathbf{B}\}$ is strongly regular at \mathbf{z} if*

$$(A.1) \quad N_{\mathbf{A}}(\mathbf{z}) \cap (-N_{\mathbf{B}}(\mathbf{z})) = \{0\}.$$

If \mathbf{A} and \mathbf{B} are sets defined in Theorem 3.3, we can prove that $N_{\mathbf{A}}(\mathbf{z}) = \{\beta\mathbf{z}\}$, where β is some real constant, and $N_{\mathbf{B}}(\mathbf{z}) = \{\mathbf{z} \in \mathbb{R}^{n+k} : \mathbf{x} = \mathbf{0}, \mathbf{y} \in \mathbb{R}^k\}$. Then we can conclude that $N_{\mathbf{A}}(\mathbf{z}) \cap (-N_{\mathbf{B}}(\mathbf{z})) = \{0\}$.

Proof. First, we will prove that the set \mathbf{B} satisfies the strongly regularity condition. Recall that $\mathbf{B} = \{\mathbf{z} \in \mathbb{R}^{n+k} : z_{n+i} = y_i, i = 1, \dots, k\}$. Since \mathbf{B} is an affine space, every limiting sequence $\{\mathbf{z}^p\} \in \mathbf{B} \rightarrow \mathbf{z}$ is equivalent to $\{\mathbf{x}^p\} \in \mathbb{R}^n \rightarrow \mathbf{x}$. Therefore, for each \mathbf{z}^p , $N_{\mathbf{B}}^{\text{prox}}(\mathbf{z}^p) = \text{cone}(\mathbb{P}_{\mathbf{B}}^{-1}(\mathbf{z}^p) - \mathbf{z}^p) = \{\tilde{\mathbf{z}} \in \mathbb{R}^{n+k} : \mathbf{x} = \mathbf{0}, \tilde{\mathbf{y}} \in \mathbb{R}^k\}$. Thus, $N_{\mathbf{B}}(\mathbf{z}) = \tilde{\mathbf{z}}$ where $\mathbf{x} = \mathbf{0}$, and $\tilde{\mathbf{y}} \in \mathbb{R}^k$.

For $\mathbf{A} = \{\mathbf{z} \in \mathbb{R}^{n+k} : |\mathbf{F}^H \mathbf{z}| = \mathbf{b}^{\frac{1}{2}}\}$, because $\mathbb{P}_{\mathbf{A}}^{-1}(\mathbf{z}) = \{\mathbf{z}_1 \in \mathbb{R}^{n+k} : \theta(\mathbf{F}^H \mathbf{z}_1) = \theta(\mathbf{F}^H \mathbf{z})\}$, where $\theta(\cdot)$ is the element-wise phase operator. The structure of set $\mathbb{P}_{\mathbf{A}}^{-1}(\mathbf{z})$ can be derived using theoretical results from [44].

LEMMA A.3. [44] *Let $\mathbf{z}_1 \in \mathbb{R}^n$ be a vector with a z -transform that has no zeros in reciprocal pairs. For any $\mathbf{z}_2 \in \mathbb{R}^n$, if $m \geq 2n - 1$ and $\theta(\mathbf{F}^H \mathbf{z}_1) = \theta(\mathbf{F}^H \mathbf{z}_2)$, then $\mathbf{z}_1 = \beta \mathbf{z}_2$ for some positive constant β .*

Recalling the Assumption 3.2, we can conclude that $\mathbb{P}_{\mathbf{A}}^{-1}(\mathbf{z}) = \{\beta\mathbf{z}, \beta > 0\}$ by using Lemma A.3. As a result, $N_{\mathbf{A}}(\mathbf{z}) = \{\alpha\mathbf{z}\}$, α is some real number. Because $\mathbf{x} \neq \mathbf{0}$, $\alpha\mathbf{z}$ cannot be lied in the $N_{\mathbf{B}}(\mathbf{z})$ only if $\alpha = 0$. As a result, $N_{\mathbf{A}}(\mathbf{z}) \cap (-N_{\mathbf{B}}(\mathbf{z})) = \{0\}$. \square

Next, the super-regularity condition will be introduced to aid in the analysis of the convergence rate of the BDR method.

DEFINITION A.4 (super-regularity). *Let Ω be a closed subset of \mathbb{R}^{n+k} . We say Ω is (ε, δ) -regular at \mathbf{z} if there exist $\varepsilon \geq 0$ and $\delta \geq 0$ such that*

$$\begin{cases} \mathbf{z}_1, \mathbf{z}_2 \in \Omega \cap \mathbb{B}_{\delta}(\mathbf{z}) \\ \mathbf{u} \in N_{\Omega}^{\text{prox}}(\mathbf{z}_1) \end{cases} \text{ leads to } \langle \mathbf{u}, \mathbf{z}_2 - \mathbf{z}_1 \rangle \leq \varepsilon \|\mathbf{u}\|_2 \cdot \|\mathbf{z}_2 - \mathbf{z}_1\|_2,$$

then we say Ω is (ε, δ) -regular at \mathbf{z} .

Moreover, if for any $\varepsilon > 0$, there exists $\delta > 0$ so that Ω is (ε, δ) -regular at \mathbf{z} , then Ω is said to be super-regular at \mathbf{z} .

Super-regularity is a property that can be thought of as a smoothness condition. In this paper, we will prove that \mathbf{A} and \mathbf{B} in Theorem 3.3 satisfy the super-regularity condition.

Proof. For any two elements \mathbf{z}_1 and \mathbf{z}_2 in \mathbf{B} , as proven above, $\mathbf{u} \in N_{\mathbf{B}}^{\text{prox}}(\mathbf{z}_1) = \{\tilde{\mathbf{z}} | \mathbf{x} = \mathbf{0}, \tilde{\mathbf{y}} \in \mathbb{R}^k\}$. As a result, $\langle \mathbf{u}, \mathbf{z}_2 - \mathbf{z}_1 \rangle = 0 \leq \varepsilon \|\mathbf{u}\|_2 \cdot \|\mathbf{z}_2 - \mathbf{z}_1\|_2$. Thus, for any $\varepsilon > 0$, there always exists $\delta > 0$, which satisfies the inequality.

Next, when \mathbf{z} satisfies the conditions in Assumption 3.2, there are at most 2^{n+k} different solutions in \mathbf{R}^{n+k} . So $|\mathbf{A}| \leq 2^{n+k}$. Therefore, there exists $\delta > 0$ such that $\mathbf{A} \cap \mathbb{B}_\delta(\mathbf{z}) = \mathbf{z}$. As a result, we can conclude that \mathbf{A} is super-regular at \mathbf{z} . The proof is complete. \square

By combining the super-regularity of feasible sets \mathbf{A} and \mathbf{B} with the strong regularity of $\{\mathbf{A}, \mathbf{B}\}$, the local R-linear convergence rate of BDR can be deduced using Theorem 4.3 in [37].

Remark: Theorem 3.3 guarantees that the sequence $\{\mathbf{z}^p\}$ converges to $\mathbf{A} \cap \mathbf{B}$. As stated in Theorem 3.1, finding the fixed points of $\mathbb{T}(\cdot)$ is sufficient to find $\mathbf{A} \cap \mathbf{B}$. Thus, we can loosen the constraints in Theorem 3.3 accordingly. This will be considered in future work. It should be noted that calculating $\mathbb{P}_{\mathbf{A}}(\mathbf{z}^{p-1})$ is difficult under these conditions and usually requires iterative algorithms such as gradient descent to approximate the projection.

Appendix B. The proof of the (3.8). We will use the techniques presented in [40] to prove (3.8). Before the proof, an important theorem will be introduced first.

THEOREM B.1. [40] *Let \mathcal{A} be a set of matrices, and let $\boldsymbol{\xi}$ be a random vector whose entries ξ_j are independent, mean-zero, variance 1, and L -subgaussian random variables. Set*

$$E = \gamma_2(\mathcal{A}, \|\cdot\|_2) (\gamma_2(\mathcal{A}, \|\cdot\|_2) + d_F(\mathcal{A})) + d_F(\mathcal{A})d_2(\mathcal{A}),$$

$$V = d_2(\mathcal{A}) (\gamma_2(\mathcal{A}, \|\cdot\|_2) + d_F(\mathcal{A})), \quad \text{and} \quad U = d_2^2(\mathcal{A})$$

Then, for $t > 0$,

$$\mathbb{P} \left(\sup_{\mathbf{A} \in \mathcal{A}} \|\mathbf{A}\boldsymbol{\xi}\|_2^2 - \mathbb{E}\|\mathbf{A}\boldsymbol{\xi}\|_2^2 \geq c_1 E + t \right) \leq 2 \exp \left(-c_2 \min \left\{ \frac{t^2}{V^2}, \frac{t}{U} \right\} \right).$$

The constants c_1 and c_2 depend only on L .

In Theorem B.1, $d_F(\mathcal{A}) := \sup_{\mathbf{A} \in \mathcal{A}} \|\mathbf{A}\|_F$, $d_2(\mathcal{A}) := \sup_{\mathbf{A} \in \mathcal{A}} \|\mathbf{A}\|_2$, and $\|\mathbf{A}\|_2 := \sup_{\|\mathbf{x}\|_2 \leq 1} \|\mathbf{A}\mathbf{x}\|_2$. $\gamma_2(\mathcal{A}, \|\cdot\|_2)$ is the γ_2 -functional of a set of matrices \mathcal{A} endowed with the operator norm, which is defined as follows.

DEFINITION B.2. [40] *For a metric space (T, d) , an admissible sequence of T is a collection of subsets of T denoted by $\{T_r : r \geq 0\}$, such that for every $s \geq 1$, $|T_r| \leq 2^{2^s}$ and $|T_0| = 1$. Then define*

$$\gamma_2(T, d) := \inf \sup_{t \in T} \sum_{r=0}^{\infty} 2^{r/2} d(t, T_r),$$

where the infimum is taken with respect to all admissible sequences of T .

To prove (3.8), we will apply Theorem B.1 to analyze $\sup_{\mathcal{A} \in \mathcal{A}} \left| \|\mathbf{A}\boldsymbol{\xi}\|_2^2 - \mathbb{E}\|\mathbf{A}\boldsymbol{\xi}\|_2^2 \right|$ when $\mathcal{A} = \{\mathbf{V}_{\mathbf{h}}, \mathbf{h} \in \mathbf{D}\}$, where $\mathbf{D} := \{\mathbf{h} \in \mathbb{R}^{n+k} : \|\mathbf{h}\|_2 \leq 1, \mathbf{h} \in \mathbf{C}_2\}$, where $\mathbf{C}_2 := \{\mathbf{h} \mid |\mathbf{F}_i^H \mathbf{h}|^2 \leq 4, i = 1, \dots, n+k\}$.

Proof. Recall that

$$\mathbf{V}_{\mathbf{h}} := \frac{1}{\sqrt{k}} \mathbf{P}_{\Omega} \mathbf{F}^{-1} \hat{\mathbf{H}} \mathbf{F}_2,$$

where \mathbf{F}_2 represents the last k columns of Fourier matrix \mathbf{F} . Using the convolutional theorem, we can obtain

$$\mathbf{F}^{-1} \hat{\mathbf{H}} \mathbf{F} = \mathbf{F}^{-1} \mathbf{F} (\mathbf{H}_{\text{circ}} \mathbf{I}) = \mathbf{H}_{\text{circ}},$$

where each row of \mathbf{H}_{circ} is a circular shift of \mathbf{h} and \mathbf{H}_{circ} is symmetry. Therefore,

$$\|\mathbf{V}_{\mathbf{h}}\|_{\mathbb{F}}^2 = \frac{1}{k} \|\mathbf{P}_{\Omega} \mathbf{F}^{-1} \hat{\mathbf{H}} \mathbf{F}_2\|_{\mathbb{F}}^2 \leq \frac{1}{k} \|\mathbf{P}_{\Omega} \mathbf{F}^{-1} \hat{\mathbf{H}} \mathbf{F}\|_{\mathbb{F}}^2 \leq \|\mathbf{h}\|_2^2 \leq 1.$$

Thus, for all $\mathbf{h} \in \mathbf{D}$, we have

$$d_F(\mathcal{A}) \leq 1.$$

At the same time, for every $\mathbf{h} \in \mathbf{D}$, we have

$$\begin{aligned} \|\mathbf{V}_{\mathbf{h}}\|_2 &= \frac{1}{\sqrt{k}} \left\| \mathbf{P}_{\Omega} \mathbf{F}^{-1} \hat{\mathbf{H}} \mathbf{F}_2 \right\|_2 \\ &\leq \frac{1}{\sqrt{k}} \|\hat{\mathbf{H}}\|_2 = \frac{1}{\sqrt{k}} \|\mathbf{h}\|_{\infty} \leq \frac{2}{\sqrt{k}}, \end{aligned}$$

where $\|\mathbf{h}\|_{\infty} := \|\mathbf{F}^H \mathbf{h}\|_{\infty}$. So for every $\mathbf{h} \in \mathbf{D}$, we have

$$d_2(\mathcal{A}) \leq \frac{2}{\sqrt{k}}.$$

The γ_2 -function can be bounded in terms of covering numbers by the well-known Dudley integral as below[40]

$$(B.1) \quad \gamma_2(\mathcal{A}, \|\cdot\|_2) \lesssim \int_0^{d_2(\mathcal{A})} \log^{1/2} N(\mathcal{A}, \|\cdot\|_2, u) du,$$

where $A \lesssim B$ means that there is an absolute constant c_1 such that $A \leq c_1 B$. For a metric space (T, d) and $u > 0$, the covering number $N(T, d, u)$ is defined as the minimum number of open balls with radius u in (T, d) required to cover T .

Because

$$\|\mathbf{V}_{\mathbf{h}_1} - \mathbf{V}_{\mathbf{h}_2}\|_2 = \|\mathbf{V}_{\mathbf{h}_1 - \mathbf{h}_2}\|_2 \leq \frac{1}{\sqrt{k}} \|\mathbf{h}_1 - \mathbf{h}_2\|_{\infty}.$$

and hence for every $u > 0$, $N(\mathcal{A}, \|\cdot\|_2, u) \leq N\left(\mathbf{D}, \frac{1}{\sqrt{k}} \|\cdot\|_{\infty}, u\right)$.

To bound the integral (B.1) above, we will divide the interval of integral into two

parts.

$$\begin{aligned}
\text{(B.2)} \quad \gamma_2(\mathcal{A}, \|\cdot\|_2) &\lesssim \int_0^{\frac{2}{\sqrt{k}}} \log^{1/2} N(\mathbf{D}, k^{-1/2} \|\cdot\|_\infty, u) \, du \\
&\lesssim \underbrace{\int_{\frac{1}{k}}^{\frac{2}{\sqrt{k}}} \log^{1/2} N(\mathbf{D}, k^{-1/2} \|\cdot\|_\infty, u) \, du}_{(1)} \\
&\quad + \underbrace{\int_0^{\frac{1}{k}} \log^{1/2} N(\mathbf{D}, k^{-1/2} \|\cdot\|_\infty, u) \, du}_{(2)}.
\end{aligned}$$

For (1), we use Lemma B.3 to bound $\log^{1/2} N(\mathbf{D}, k^{-1/2} \|\cdot\|_\infty, u) \, du$ in the interval $[\frac{1}{k}, \frac{2}{\sqrt{k}}]$.

LEMMA B.3. [40] *There exists an absolute constant c for which the following holds. Let X be a normed space, consider a finite set $\mathcal{U} \subset X$ of cardinality N , and assume that for every $L \in \mathbb{N}$ and $(\mathbf{u}_1, \dots, \mathbf{u}_L) \in \mathcal{U}^L$, $\mathbb{E}_\epsilon \left\| \sum_{j=1}^L \epsilon_j \mathbf{u}_j \right\|_X \leq A\sqrt{L}$, where $(\epsilon_j)_{j=1}^L$ denotes a Rademacher vector. Then for every $u > 0$,*

$$\log N(\text{conv}(\mathcal{U}), \|\cdot\|_X, u) \leq c(A/u)^2 \log N.$$

The proof of Lemma B.3 can be shown in [40]. It is applied for the set

$$\mathcal{U} = \left\{ \pm\sqrt{2}e_1, \dots, \pm\sqrt{2}e_{n+k} \right\}.$$

where the e_i are the standard basis vectors. Noting that $\mathbf{D} \subset \mathbf{B}_2^{n+1} \subset \text{conv}(\mathcal{U})$ and that we may choose $A = c\sqrt{\log(n+k)}$, so we have

$$\begin{aligned}
\log N(\mathbf{D}, k^{-1/2} \|\cdot\|_\infty, u) &\leq \log N(\text{conv}(\mathcal{U}), k^{-1/2} \|\cdot\|_\infty, u) \\
\text{(B.3)} \quad &\lesssim \left(\frac{1}{u\sqrt{k}} \right)^2 \log^2(n+k).
\end{aligned}$$

Using the bound (B.3) to calculate part (2) will result in an improper integral. Therefore, we need to provide a new bound of $\log N(\mathbf{D}, k^{-1/2} \|\cdot\|_\infty, u)$. To do so, we apply the standard volumetric argument and obtain the following lemma:

LEMMA B.4. *Let $\|\cdot\|$ be some semi-norm on \mathbb{R}^n and let U be a subset of the unit ball \mathbf{B}_1^n . Then the covering numbers satisfy, for $t > 0$,*

$$N(U, \|\cdot\|, t) \leq \left(1 + \frac{2}{t} \right)^n.$$

Because $\mathbf{D} \subset \mathbf{B}_2^{n+k} \subset \mathbf{B}_1^{n+k}$, and $k^{-1/2} \|\cdot\|_\infty$ is a semi-norm, we have

$$\text{(B.4)} \quad \log N(\mathbf{D}, k^{-1/2} \|\cdot\|_\infty, u) \lesssim (n+k) \log\left(1 + \frac{2}{u}\right).$$

Combing (B.3) and (B.4) into (B.2), we have

$$\begin{aligned}
\gamma_2(\mathcal{A}, \|\cdot\|_2) &\lesssim \int_0^{d_2(\mathcal{A})} \log^{1/2} N(\mathbf{D}, k^{-1/2} \|\cdot\|_\infty, u) du \\
&\lesssim \int_{\frac{1}{k}}^{\frac{2}{\sqrt{k}}} \log^{1/2} N(\mathbf{D}, k^{-1/2} \|\cdot\|_\infty, u) du \\
&\quad + \int_0^{\frac{1}{k}} \log^{1/2} N(\mathbf{D}, k^{-1/2} \|\cdot\|_\infty, u) du \\
&\lesssim \int_{\frac{1}{k}}^{\frac{2}{\sqrt{k}}} \left(\frac{1}{u\sqrt{k}} \right) \log(n+k) du \\
&\quad + \sqrt{(n+k)} \int_0^{\frac{1}{k}} \sqrt{\log\left(1 + \frac{2}{u}\right)} du \\
\text{(B.5)} \quad &\lesssim \frac{\log(n+k) \log(2\sqrt{k})}{\sqrt{k}} + \frac{\sqrt{n+k}}{\sqrt{2k}} \sqrt{\log(e(1+2k))},
\end{aligned}$$

where the inequality of $\int_0^{\frac{1}{k}} \sqrt{\log\left(1 + \frac{2}{u}\right)} du$ above is held by the Cauchy-Schwarz.

$$\int_0^{\frac{1}{k}} \sqrt{\log\left(1 + \frac{2}{u}\right)} du \leq \sqrt{\int_0^{\frac{1}{k}} 1 du \int_0^{\frac{1}{k}} \log\left(1 + \frac{2}{u}\right) du} = \frac{1}{\sqrt{k}} \sqrt{\int_0^{\frac{1}{k}} \log\left(1 + \frac{2}{u}\right) du}.$$

A change of variables and integration by parts yields

$$\begin{aligned}
\int_0^{\frac{1}{k}} \log\left(1 + \frac{2}{u}\right) du &= \frac{1}{2} \int_k^\infty t^{-2} \log(1+2t) dt \\
&= -\frac{1}{2} t^{-1} \log(1+2t) \Big|_k^\infty + \int_k^\infty \frac{1}{2t^2+t} dt \\
&\leq \frac{1}{2k} \log(1+2k) + \int_k^\infty \frac{1}{2t^2} dt \\
&= \frac{1}{2k} \log(e(1+2k)).
\end{aligned}$$

Using L'Hospital's rule, we can derive that $\lim_{k \rightarrow +\infty} \gamma_2(\mathcal{A}, \|\cdot\|_2) = 0$. Therefore, for any $\delta > 0$, as long as k is sufficiently large, we can guarantee that $\gamma_2(\mathcal{A}, \|\cdot\|_2) \lesssim \frac{\sqrt{\delta}}{2}$ for the given value of k . Define

$$f(k) := \frac{\log(n+k) \log(2\sqrt{k})}{\sqrt{k}} + \frac{\sqrt{n+k}}{\sqrt{2k}} \sqrt{\log(e(1+2k))}.$$

We plot the $f(k)$ in Fig.14, where k/n increases from 1 to 10 with an interval of 1, and n varies from 1000 to 10000. We can find that $f(k) < 1$ as long as k/n is large enough.

Using the definition of E , we can derive that $\lim_{k \rightarrow +\infty} E = 0$. Therefore, by properly choosing the constant c in Theorem 3.9 such that k is sufficiently large, we have:

$$E \leq \frac{\delta}{4c_1},$$

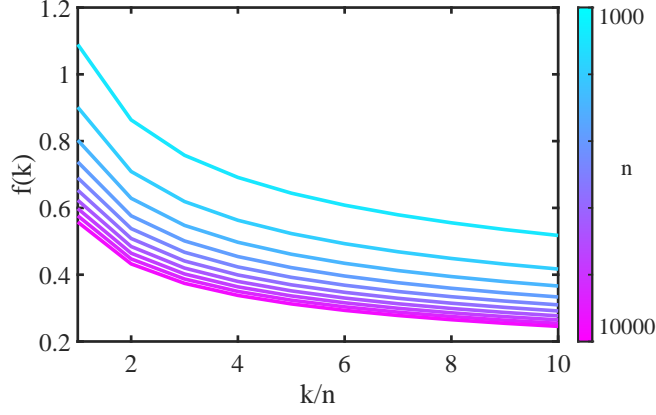


Fig. 14: The plot shows $f(k)$ as k/n increases from 1 to 10 with an interval of 1, and n varies from 1000 to 10000.

where E and c_1 are chosen as in Theorem B.1. By Theorem B.1 and let $t = \delta/4$, we obtain

$$\mathbb{P}\left(\delta_s \geq \frac{\delta}{2}\right) \leq \mathbb{P}\left(\delta_s \geq c_1 E + \delta/4\right) \leq \exp\left(-c_2 \left(\frac{k\delta^2}{16(\sqrt{\delta} + 2)^2}\right)\right) \leq \eta,$$

which completes the proof after possibly increasing the value of c sufficiently to compensate for c_2 . \square

Appendix C. The proof of the (3.9). Next, we will evaluate that

$$\sup_{\mathbf{h} \in \mathcal{C}_2} \left| \frac{1}{k} \left(\mathbf{P}_\Omega \mathbf{F}^{-1} \hat{\mathbf{H}} \mathbf{F}_1 \mathbf{x} \right)^H \mathbf{P}_\Omega \mathbf{F}^{-1} \hat{\mathbf{H}} \mathbf{F}_2 \mathbf{y} \right|.$$

By the Chebyshev inequality, we can conclude that

$$\begin{aligned} \mathbb{P}\left(\left| \frac{1}{k} \left(\mathbf{P}_\Omega \mathbf{F}^{-1} \hat{\mathbf{H}} \mathbf{F}_1 \mathbf{x} \right)^H \mathbf{P}_\Omega \mathbf{F}^{-1} \hat{\mathbf{H}} \mathbf{F}_2 \mathbf{y} \right| \geq \frac{\delta}{2}\right) &\leq \frac{4 \left\| \left(\mathbf{P}_\Omega \mathbf{F}^{-1} \hat{\mathbf{H}} \mathbf{F}_2 \right)^H \mathbf{P}_\Omega \mathbf{F}^{-1} \hat{\mathbf{H}} \mathbf{F}_1 \mathbf{x} \right\|_2^2}{\sigma^2 k^2} \\ &\leq \frac{64 \|\mathbf{x}\|_2^2}{\delta^2 k^2} \leq \eta. \end{aligned}$$